



Natural Resources
Canada Ressources naturelles
Canada

**GEOLOGICAL SURVEY OF CANADA
OPEN FILE 7666**

**Alteration proximal to the sharp-walled
Cu-(Ni)-PGE vein footwall mineralization of the
Podolsky deposit, Sudbury Ontario**

L.M. MacInnis, D.J. Kontak, D.E. Ames, and N.L. Joyce

2014

Canada



GEOLOGICAL SURVEY OF CANADA OPEN FILE 7666

Alteration proximal to the sharp-walled Cu-(Ni)-PGE vein footwall mineralization of the Podolsky deposit, Sudbury, Ontario

L.M. MacInnis¹, D.J. Kontak¹, D.E. Ames², and N.L. Joyce²

¹Laurentian University, Sudbury, Ontario

²Geological Survey of Canada, Ottawa, Ontario

2014

© Her Majesty the Queen in Right of Canada, as represented by the Minister of Natural Resources Canada, 2014

doi:10.4095/295482

This publication is available for free download through GEOSCAN (<http://geoscan.nrcan.gc.ca/>)

Recommended citation

MacInnis, L.M., Kontak, D.J., Ames, D.E., and Joyce, N.L., 2014. Alteration proximal to the sharp-walled Cu-(Ni)-PGE vein footwall mineralization of the Podolsky deposit, Sudbury, Ontario; Geological Survey of Canada, Open File 7666, 1 zip file. doi:10.4095/295482

Publications in this series have not been edited; they are released as submitted by the author.

Contribution to the Geological Survey of Canada's Targeted Geoscience Initiative 4 (TGI-4) Program (2010-2015)

TABLE OF CONTENTS

Background	1
Introduction	1
Mapping of the Grey Gabbro	1
Sampling and whole rock geochemistry	3
Methods and results	3
Mineral geochemistry	3
Isotope geochemistry	4
<i>Oxygen isotopes</i>	4
<i>Strontium isotopes</i>	4
<i>Sulphur isotopes</i>	4
$^{40}\text{Ar}/^{39}\text{Ar}$ geochronology	12
<i>Results</i>	14
Summary	15
Acknowledgments	15
References	15
Appendices	

 Appendix A. Descriptions and locations of samples used in this study

 Appendix B. Mineral chemical database including
 1) analytical standards and operating conditions
 2) pyroxene analysis, n=34
 3) amphibole analysis, n=23
 4) biotite analysis, n=20
 5) chlorite analysis, n=3

 Appendix C. $^{40}\text{Ar}/^{39}\text{Ar}$ actinolite analytical data of sample LM-P-060

Figures

Figure 1. Regional map of the Sudbury Structure showing the location of the Podolsky deposit	2
Figure 2. Cross-section of the Podolsky deposit showing the 2000 deposit and the Whistle embayment	2
Figure 3. Photographs of chalcopyrite mineralization in grey gabbro	3
Figure 4. Schematic diagram of Podolsky grey gabbro showing the distribution of epidote alteration and the development of foliation relative to Cu-Ni-PGE mineralization	4
Figure 5. Photographs of actinolite along the contact of grey gabbro and a chalcopyrite vein	12
Figure 6. $^{40}\text{Ar}/^{39}\text{Ar}$ step-heating data plots	13
Figure 7. $^{40}\text{Ar}/^{39}\text{Ar}$ single fusion data plots	14

Tables

Table 1. Bulk rock, oxygen and strontium isotope geochemistry, Podolsky deposit (of_7666-Table1.xls)	5
Table 2. Petrography and modal mineralogy of the chalcopyrite-rich ore, altered grey gabbro, and less altered grey gabbro in the Podolsky deposit (of_7666-Table2.xls)	9
Table 3. $\delta^{34}\text{S}$ analyses of chalcopyrite from levels 1700, 1850, 1950, and 2225 of the Podolsky mine (of_7666-Table3.xls)	12

Alteration proximal to the sharp-walled Cu-(Ni)-PGE vein footwall mineralization of the Podolsky deposit, Sudbury, Ontario

L.M. MacInnis¹, D.J. Kontak¹, D.E. Ames², and N.L. Joyce²

¹Department of Earth Sciences, Laurentian University, Sudbury, Ontario P3E 2C6

²Geological Survey of Canada, 601 Booth Street, Ottawa, Ontario K1A 0E8

BACKGROUND

The footwall of the Sudbury Igneous Complex (SIC) hosts high-grade Cu-(Ni)-PGE deposits that have recently become prime exploration targets due to the increase in metal prices and the depletion in the mature mining district of historically nickel-rich contact deposits. These footwall deposits differ in their setting, composition, and vein-like geometry from traditional Ni-Cu-Co-rich contact ore deposits. Footwall SIC mineralization is known for its sharp-walled nature and, in some cases, the apparent absence of intense alteration. In other cases, deposits such as Podolsky are enveloped by intense alteration (e.g. epidote, actinolite, and magnetite). This alteration could provide a significantly larger target for exploration if the alteration can be unambiguously characterized as a vector to sulphide mineralization.

The project was designed to identify the nature, origin, significance, and relevance of alteration in SIC mineralization at the Podolsky deposit. It was funded by the Geological Survey of Canada as part of the Targeted Geoscience Initiative 4 program (TGI4): Ni-Cu-PGE-Cr Project (Ames and Houlé, 2011; Ames et al., 2012) and is part of a M.Sc. project at Laurentian University (Sudbury, Canada; LU) by L.M. MacInnis under the supervision of Drs. D.J. Kontak (LU) and D.E. Ames (GSC). This study documents the variation of the alteration minerals within the “grey gabbro” wall rock with proximity to the sharp-walled chalcopyrite vein of the Podolsky deposit. By constraining the nature, origin, and significance of alteration in the Sudbury Igneous Complex (SIC) footwall mineralization, a larger target area for footwall-style deposits can be delineated. Included with this report is a geochemical databases consisting of underground and drill core samples from multiple transects and intensely altered samples of grey gabbro from adjacent to the sharp-walled veins.

The data and results of this study are presented here whereas the interpretations will be released in journal papers.

INTRODUCTION

The Podolsky Cu-(Ni)-PGE deposit, which is situated in Wisner township (~35 kilometres north-northeast of Sudbury, is hosted by the Whistle-Parkin radial offset

of the Paleoproterozoic 1850 Ma (Krogh et al., 1984) Sudbury Igneous Complex (SIC; Fig. 1). The Podolsky mine produced ~1.5 Mt of 4.29% Cu, 0.38% Ni, 0.051 oz/t Pt, 0.054 oz/t Pd, and 0.024 oz/t Au, between 2007 and 2011 (Holly Davidson; pers. comm.). The Podolsky deposit is situated ~650 m below the Ni-Cu-Co Whistle deposit, which is at the intersection of the basal contact of the SIC and the offset structure (Fig. 2). Podolsky is a hybrid deposit that displays “sharp-walled” and “low-sulphide” elements of footwall mineralization systems in the 2000 deposit zone (Farrow et al., 2005). The northeast-trending Whistle-Parkin offset is atypical as it contains intrusive phases, such as leucocratic quartz diorite (LQD) and quartz diorite (QD), as well as the inclusion of QD (IQD) as pods within metabreccia (MTBX). This study is focused on the grey gabbro unit: a large (230 m by 270 m) uniform rock fragment that hosts large (<1 m) sharp-walled veins, many of which contain epidote-actinolite-magnetite-bearing alteration halos.

Thus, alteration-specific mineralization at the Podolsky deposit, which can be fully characterized and chemically fingerprinted, may provide criteria for vectoring towards mineralization in other, more complex areas.

- The first objective was to determine the mineralogy and geochemistry of the least-altered gabbroic host rock to the Podolsky copper-palladium mineralization. This characterization of the least altered host rock will allow documentation of the macro- and micro-scale changes in rock texture, mineralogy, and chemistry due to fluid–rock interaction (i.e. the interaction of the mineralizing fluids with the relatively uniform medium).
- The second and most important objective was to assess the nature and origin of the alteration that was variably associated with the ore zones within this unit and compare this to the alteration present in the footwall environment of the SIC. The characterization and chemical fingerprinting of alteration-specific mineralization could provide criteria for targeting mineralization in other footwall environments.

MAPPING OF THE GREY GABBRO

The grey gabbro unit was remapped using the KGHM International archived photo library of 12 drill-holes (FNX40065, FNX4121, FNX4134B, FNX4134,

Alteration proximal to the sharp-walled Cu-(Ni)-PGE vein footwall mineralization of the Podolsky deposit, Sudbury

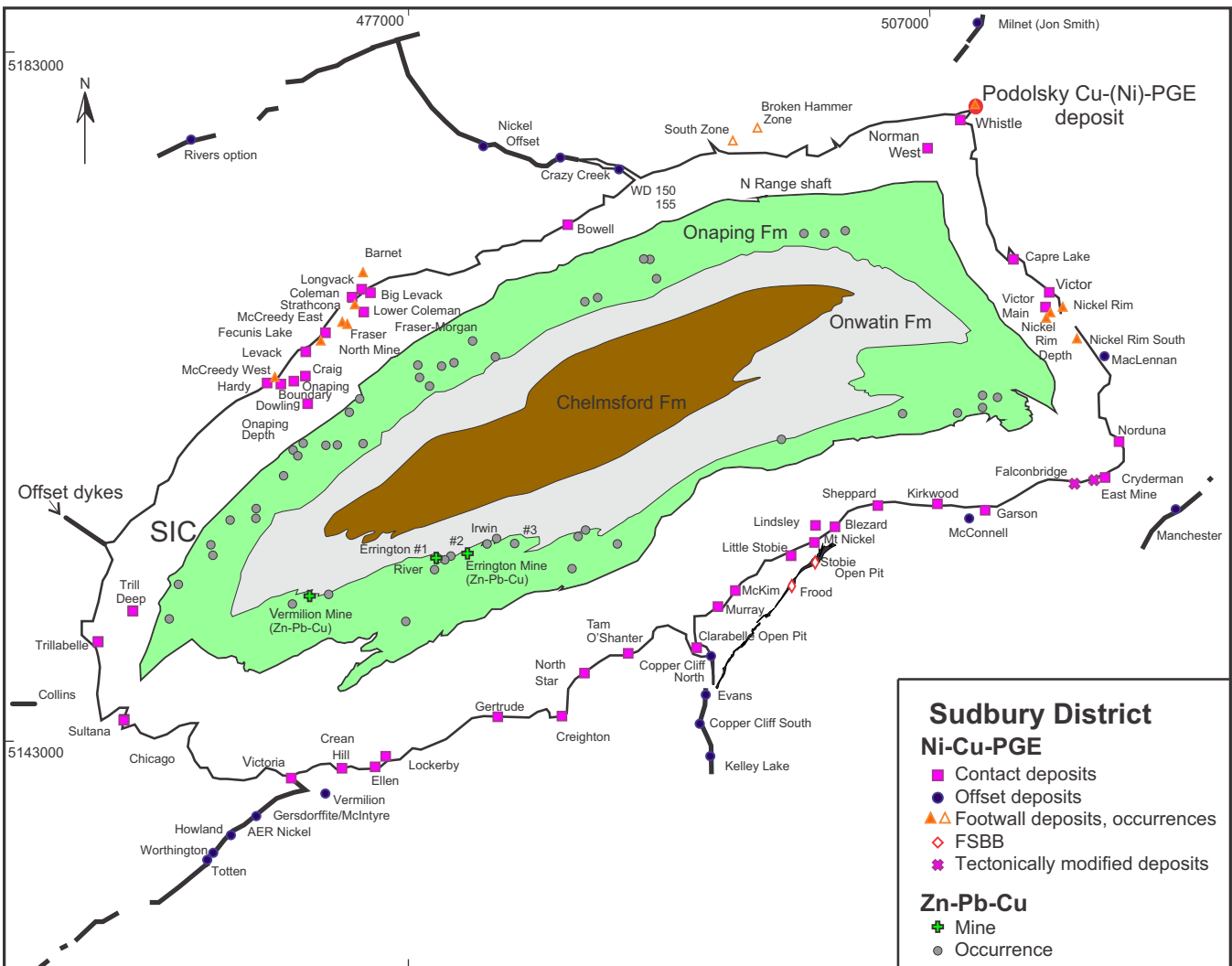


Figure 1. Regional map of the Sudbury Structure (SS). The location of the Podolsky deposit is located in the North Range of the SS, within the Whistle-Parkin radial offset. The red circle indicates the location of the Podolsky deposit. Modified from Ames and Farrow (2007). Fm = Formation.

FNX4307, FNX4332, FNX4355, FNX4363, FNX4054, FNX4514, FNX4605, and FNX4993) that intersected the unit vertically and horizontally. Drillholes were selected according to their spatial location within the unit using a 3-D-modelling program Datamine Studio 3, which orients drillholes based on their surveyed location and dip. Diamond drillholes were also targeted according to their availability.

The grey gabbro unit was mapped in 5 ft intervals based on lithology, texture, fabric, mineralization, and alteration assemblages. In order to assess the homogeneity of the unit, major and minor lithologies were identified using colour index as proxy for composition, and grain size as a proxy of possible proximity to contacts. The degree of alignment of plagioclase laths was used to measure the structural fabric (i.e. foliation) within the unit. Mineralization was also considered as a lithology and separated into massive (100–85 % chalcopyrite over 10 cm) or semi-massive (85–55 % chal-

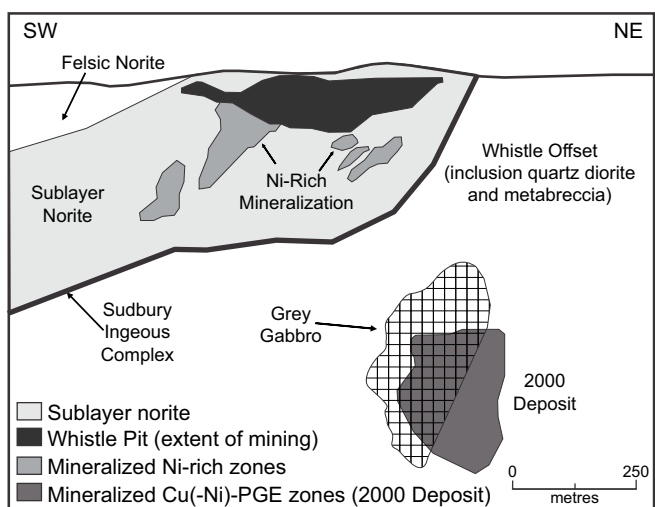


Figure 2. Cross-section of the Podolsky deposit, looking northwest. Note the location of the Podolsky 2000 deposit in relation to the Whistle embayment. Modified from Farrow et al. (2005).

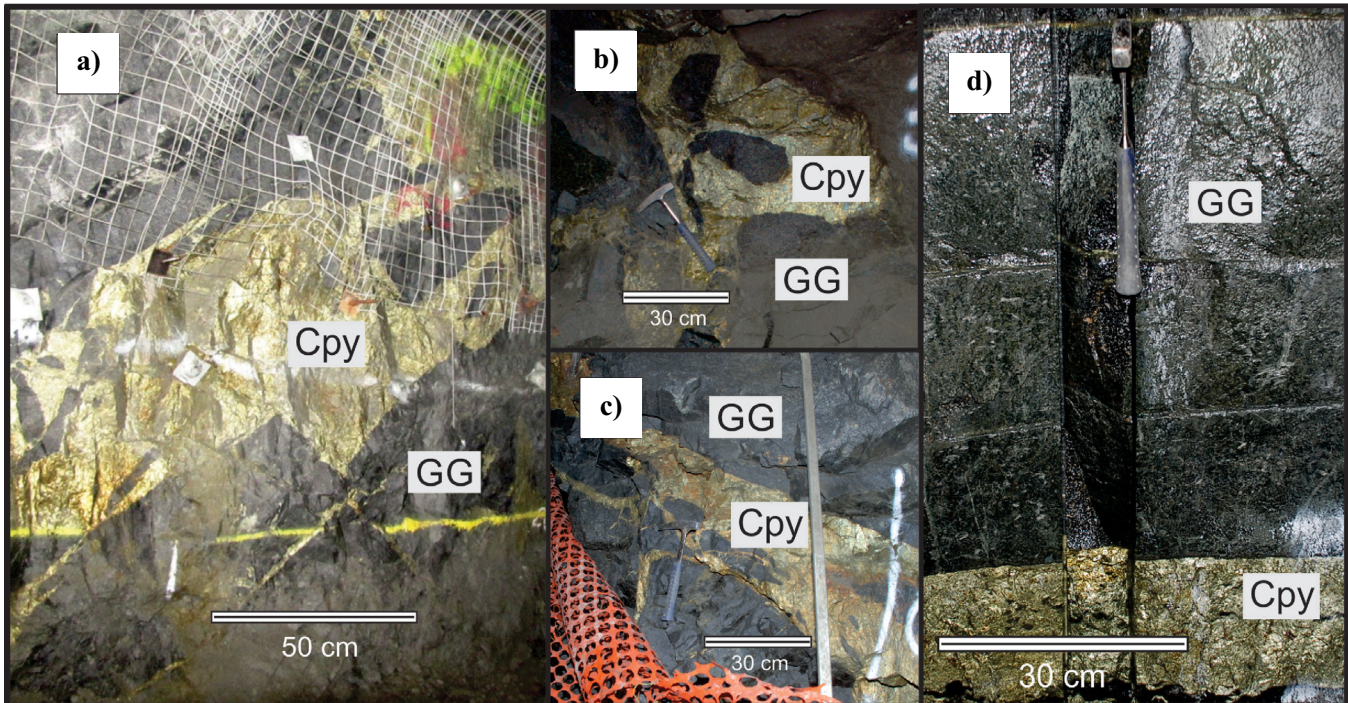


Figure 3. Structurally controlled veins at the Podolsky mine, which are hosted by grey gabbro (GG): **a)** sharp-walled chalcopyrite (Cpy) mineralization hosted by grey gabbro on the 1925 level; **b)** grey gabbro clasts captured within a chalcopyrite vein on the 2225 level; **c)** sharp-walled veining with small grey gabbro clasts captured within the chalcopyrite vein on the 2000 level; **d)** grey gabbro with alteration-trends leading up to the sharp-walled chalcopyrite vein in transect LM-P-043 cut out of the 2225 level drift.

chalcopyrite over 4 in) sulphide (Fig. 3). Where minor amounts of sulphide mineralization occurred (i.e. <4 in), the interval was noted to contain chalcopyrite stringers. These stringers were further divided into >5% sulphide, or <5% sulphide. Epidote, chlorite, hematite, quartz, carbonate, and talc alteration were observed in varying degrees and intensities (i.e. low, medium, high).

These new observations were integrated with the original dataset constraints present in the Datamine Studio 3 program and then re-projected onto the original model to produce a new map for the Podolsky grey gabbro (Fig. 4).

METHODS AND RESULTS

Sampling and Whole Rock Geochemistry

Seventy samples, comprising 19 least altered, 30 altered, and 21 mineralized samples, were collected underground between levels 1700 and 2450 (Fig. 3). These were augmented with KGHM's existing collection of altered drill core samples (Appendix A).

Bulk rock geochemistry samples from this project were analyzed using standard methods by 3 laboratories: Geoscience Laboratories (GeoLabs) in Sudbury (Ontario), ACME Labs in Vancouver (British Columbia), and ActLabs in Ancaster (Ontario). Whole rock major and trace element geochemistry of 21 samples (Table 1) was performed by ACME Laboratories. The following analytical procedures were completed:

fusion digestion, followed by whole rock X-ray fluorescence for whole rock data; ICP-MS analysis after ultra-trace aqua regia digestion for precious and base metals data; ICP-MS after a lithium metaborate / tetraborate fusion and nitric acid digestion for rare earth and refractory elements; LECO analysis for carbon and sulphur; and single element analysis for FeO. An additional 30 samples were analyzed by Actlabs using the following methods: fusion digestion followed by ICP-OES for whole rock data and rare earth elements; ICP-ISE for fluorine; ICP-MS for trace elements; INAA for chlorine and nickel; fire assay followed by ICP-MS for gold, palladium, and platinum; infrared absorption for carbon and sulphur; and total iron in concentrate by titration. Six samples were analyzed by GeoLabs using the following analytical procedures: aqua regia digest followed by ICP-MS for whole rock and metal analyses; closed multi-acid digestion followed by ICP-MS for trace elements; XRF using pressed pellets for a select number of trace elements; atomic absorption to measure spikes in base metals; and infrared absorption via combustion for carbon dioxide and sulphur.

Mineral Geochemistry

Representative samples of least altered grey gabbro were studied in detail using both transmitted and reflected light microscopy and scanning electron

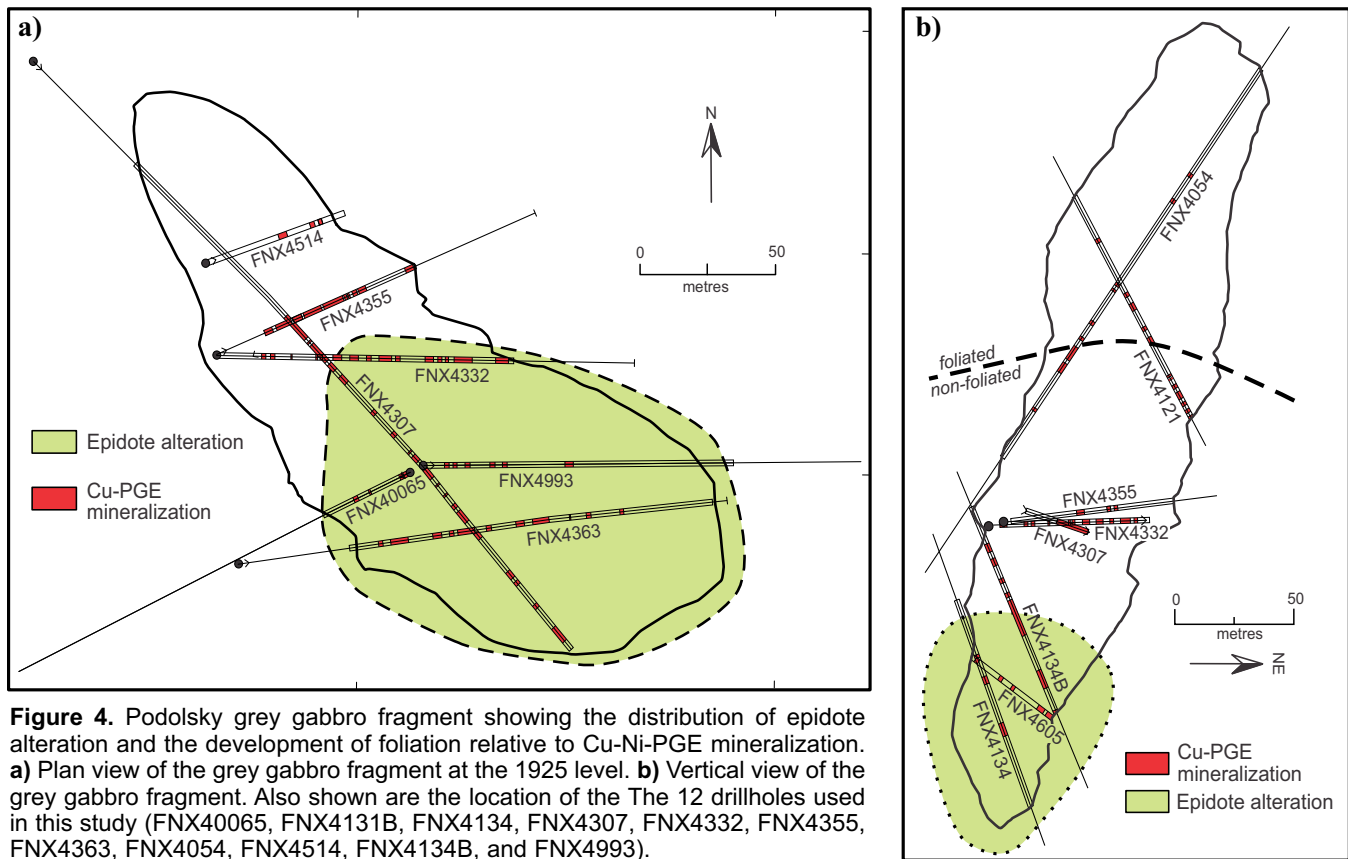


Figure 4. Podolsky grey gabbro fragment showing the distribution of epidote alteration and the development of foliation relative to Cu-Ni-PGE mineralization. **a)** Plan view of the grey gabbro fragment at the 1925 level. **b)** Vertical view of the grey gabbro fragment. Also shown are the location of the The 12 drillholes used in this study (FNX40065, FNX4131B, FNX4134, FNX4307, FNX4332, FNX4355, FNX4363, FNX4054, FNX4514, FNX4134B, and FNX4993).

microscopy with an energy dispersive system (SEM-EDS) (Table 2). For the latter, a JEOL 6400 SEM-EDS system was used, which is housed in the Central Analytical Facilities (CAF) at Laurentian University, Sudbury, Ontario with the following operating conditions: accelerating voltage of 15 kV, 1.005 nA beam current, acquisition count times of 60 s, and a working distance of 15 mm. Well characterized jadeite, diopside, orthoclase, corundum, quartz, chalcopyrite, and pyrophanite were used as standards.

Microanalyses of mafic minerals within the grey gabbro unit were obtained by wavelength-dispersive spectrometry using a Cameca SX-100 Electron Probe Micro Analyzer (EPMA) and a variety of mineral standards; the system is housed at the Ontario Geological Survey Geoscience Laboratories (Geolabs). Operation parameters were set at accelerating voltages of 20 kV with a beam current of 20 nA for clinopyroxene, amphibole, biotite, and chlorite. A focused beam was used for all mafic phases, with the exception of biotite where a defocused beam was used. The silicate mineral chemistry is provided in Appendix B.

Isotope Geochemistry

Oxygen Isotope

A total of 20 samples, consisting of 19 whole rocks and one actinolite separate sample, were analyzed for $\delta^{18}\text{O}$

measurements at the Queen's University Facility for Isotopic Analysis in Kingston, Ontario (Table 1). Samples were liberated using BrF₅, following the standard method of Clayton and Mayeda (1963), and abraded, following the Mattinson (2005) method. Analyses were performed using a Thermo-Finnigan MAT 253 and a DELTAplusXP stable isotope ratio mass spectrometer. Analytical uncertainty was less than ± 0.1 per mil and sample reproducibility was ± 0.02 per mil.

Strontium Isotope

Three samples were analyzed for $^{87}\text{Sr}/^{86}\text{Sr}$ isotopes: an actinolite mineral separate and two least altered grey gabbro whole rock samples (Fig. 5). Strontium isotopes were analyzed with a ThermoFinnigan Triton T1 thermal ionization mass spectrometer at Carleton University's Isotope Geochemistry and Geochronology Research Centre in Ottawa, Ontario (Table 1).

Sulphur Isotope

A comprehensive suite of 15 chalcopyrite samples were collected from massive chalcopyrite sharp-walled vein transects within grey gabbro (host rock) at 4 specific regions of the mine (1700L, 1850L, 1925L, and 2225L; Table 3). Three isotope samples, on average, were collected at each site from vein contacts as well as from the middle of the vein. To avoid contamination, chalcopyrite samples were crushed into pebbles, hand-

Table 1. Bulk rock, oxygen and strontium isotope geochemistry, Podolsky Cu-(Ni)-PGE deposit.

	Method	LLD	LM-P-019	LM-P-021	LM-P-025	LM-P-028	LM-P-030	LM-P-032A	LM-P-033	LM-P-036	LM-P-037	LM-P-038	LM-P-042	LM-P-039A
Laboratory			ACME	ACME	ACME	ACME	ACME	ACME	ACME	ACME	ACME	ACME	ACME	ACME
wt%														
SiO ₂	WR-XRF	0.10	50.00	51.30	51.10	50.90	50.20	49.70	49.80	51.60	50.10	49.80	52.10	49.50
TiO ₂	WR-XRF	0.01	1.36	1.07	1.00	1.10	1.39	1.30	1.25	1.06	1.39	1.30	1.46	1.51
Al ₂ O ₃	WR-XRF	0.01	16.50	16.83	16.15	16.58	15.50	16.23	15.89	15.25	16.04	16.25	15.61	16.38
FeO ^T	WR-XRF	0.01	10.16	9.33	9.34	9.30	10.36	10.45	10.20	10.51	10.67	10.07	8.44	9.92
FeO	WR-XRF	0.01	9.819	9.018	9.027	8.991	10.017	10.098	9.864	10.161	10.314	9.738	8.154	9.594
Fe ₂ O ₃	WR-XRF	0.01	1.09	1.00	1.00	1.00	1.11	1.12	1.10	1.13	1.15	1.08	0.91	1.07
MgO	WR-XRF	0.01	5.28	5.91	6.61	6.13	6.05	5.84	5.97	6.94	5.04	5.32	7.05	5.93
MnO	WR-XRF	0.01	0.14	0.13	0.15	0.14	0.14	0.15	0.15	0.14	0.16	0.14	0.14	0.16
CaO	WR-XRF	0.01	7.82	8.40	8.30	7.95	5.91	8.02	7.49	5.18	6.89	7.31	7.84	7.57
Na ₂ O	WR-XRF	0.01	3.91	3.94	3.50	3.64	4.68	3.62	3.58	4.25	3.17	3.23	3.47	4.23
K ₂ O	WR-XRF	0.01	1.75	1.31	1.74	2.00	1.98	1.75	1.94	1.15	2.90	2.94	1.68	0.76
P ₂ O ₅	WR-XRF	0.01	0.73	0.66	0.52	0.57	0.82	0.73	0.69	0.66	0.74	0.67	0.47	0.81
LOI			1.44	0.84	1.03	1.24	2.49	1.09	1.57	2.80	1.82	1.63	1.79	2.41
Total			98.38	99.57	99.09	98.99	97.77	98.54	97.69	97.49	97.86	97.75	98.28	97.42
TOT/C	LECO	0.02	0.06	0.02	0.03	0.03	0.10	0.03	0.06	<0.02	0.06	0.06	0.06	0.03
FeO	S.E.-Assay	0.01	6.48	5.70	6.14	6.13	6.23	6.93	7.00	7.85	7.06	6.81	6.68	7.00
TOT/S	LECO	0.02	0.21	0.21	0.21	0.17	0.22	0.25	0.19	0.14	0.30	0.19	0.15	0.20
Cl														
F														
ppm														
B	ICP-MS	1.00	1	<1	<1	3	2	1	2	<1	<1	<1	2	1
Li	ICP-MS	0.10	20.3	18.2	20.7	20.4	34.2	17.5	26.3	17.2	20.4	17.1	18.5	14.3
ppb														
Se	ICP-MS	100.00	0.00	0.00	100.00	0.00	200.00	200.00	300.00	600.00	200.00	200.00	200.00	200.00
Au	ICP-MS	0.50	<0.5	<0.5	<0.5	0.60	<0.5	<0.5	<0.5	1.60	3.20	0.80	3.10	2.00
Pd	ICP-MS	10.00	<10	<10	<10	<10	<10	<10	<10	<10	<10	<10	<10	<10
Pt	ICP-MS	2.00	<2	<2	<2	<2	<2	<2	<2	<2	<2	<2	2.00	<2
Ag	ICP-MS	2.00	143	209	297	494	113	305	1275	542	247	522	358	1090
Re	ICP-MS	1	<1	<1	<1	<1	<1	<1	<1	<1	<1	<1	<1	<1
ppm														
Cu	ICP-MS	0.01	38.30	49.00	47.20	245.20	56.90	48.90	1613.10	1088.40	2887.60	2149.00	361.40	1572.80
Ni	ICP-MS	0.10	43.90	63.20	70.00	63.90	42.10	58.30	55.30	716.70	62.40	49.80	72.40	54.80
Co	ICP-MS	0.20	33.70	34.00	37.10	35.00	32.10	36.50	35.60	41.10	32.30	32.70	34.40	36.80
Cr	ICP-MS	0.50	45.10	80.80	84.60	82.40	39.70	59.40	75.70	63.80	49.90	56.60	103.60	59.30
Mn	ICP-MS	1.00	280	178	236	265	240	243	315	680	454	414	355	528
Zn	ICP-MS	1.00	94.00	65.00	86.00	86.00	71.00	94.00	88.00	127.00	107.00	96.00	77.00	112.00
Sn	ICP-MS	1.00	1	1	1	1	<1	1	2	4	1	<1	<1	<1
Ga	ICP-MS	0.50	20.1	19.4	18.8	19.5	18.8	19.6	20	16.5	22.3	20.5	17.1	18.6
Ge	ICP-MS	0.10	0.1	0.1	<0.1	<0.1	<0.1	0.1	<0.1	0.1	<0.1	0.1	0.1	0.1
In	ICP-MS	0.02	<0.02	<0.02	<0.02	<0.02	<0.02	<0.02	<0.02	<0.02	<0.02	<0.02	<0.02	<0.02
Cd	ICP-MS	0.01	0.18	0.56	1.03	2.07	0.02	0.62	0.36	0.12	0.08	0.08	0.21	0.12
La	ICP-MS	0.10	96.00	76.40	68.00	74.40	82.90	82.80	81.60	90.50	91.20	93.80	64.10	95.80
Ce	ICP-MS	0.10	186.20	154.00	134.90	149.80	169.30	165.50	162.20	180.80	181.90	181.50	126.30	189.60
Pr	ICP-MS	0.02	21.67	17.77	16.38	17.92	20.64	19.86	19.44	21.08	21.56	21.60	14.90	22.66
Nd	ICP-MS	0.30	76.60	67.10	65.60	67.30	78.20	73.20	72.30	75.70	79.10	78.30	54.20	83.50
Sm	ICP-MS	0.05	11.90	10.48	9.77	9.84	11.97	11.48	11.07	11.64	13.13	11.91	9.00	13.15
Eu	ICP-MS	0.02	3.01	2.47	2.47	2.53	2.83	2.92	2.77	2.51	2.77	2.91	2.21	2.72
Gd	ICP-MS	0.05	8.26	7.30	6.83	7.10	8.32	8.16	7.76	8.14	9.91	8.45	6.28	9.05
Tb	ICP-MS	0.01	0.91	0.80	0.76	0.81	0.95	0.90	0.87	0.89	1.11	0.95	0.67	1.00
Dy	ICP-MS	0.05	4.63	3.82	3.99	4.10	4.93	4.59	4.65	4.42	5.56	4.67	3.52	5.09
Ho	ICP-MS	0.02	0.73	0.68	0.70	0.70	0.76	0.72	0.73	0.70	0.97	0.78	0.58	0.78
Er	ICP-MS	0.03	1.98	1.75	1.91	1.77	1.91	1.98	1.97	1.71	2.82	2.16	1.56	2.21
Tm	ICP-MS	0.01	0.28	0.25	0.23	0.24	0.27	0.27	0.25	0.26	0.37	0.30	0.22	0.28
Yb	ICP-MS	0.05	1.79	1.48	1.54	1.47	1.79	1.60	1.56	1.70	2.40	1.88	1.35	1.86
Lu	ICP-MS	0.01	0.24	0.21	0.21	0.21	0.25	0.24	0.23	0.23	0.32	0.26	0.19	0.25
Zr	ICP-MS	0.10	284.90	215.60	224.80	239.10	241.40	251.60	246.10	115.80	311.90	303.40	189.10	310.40
Ba	ICP-MS	1.00	1222.00	960.00	1003.00	1097.00	1111.00	1173.00	1233.00	295.00	1308.00	1758.00	900.00	842.00
Pb	ICP-MS	0.10	13.30	23.90	55.10	37.50	3.00	20.10	17.50	3.50	3.60	9.00	15.10	6.40
Th	ICP-MS	0.20	4.50	1.80	1.90	2.00	3.60	2.30	2.60	5.50	4.80	6.40	1.80	4.00
U	ICP-MS	0.10	0.10	0.20	0.10	0.10	0.40	0.10	0.20	0.20	0.30	0.50	0.20	0.20
Bi	ICP-MS	0.02	0.05	<0.02	0.09	0.13	<0.02	<0.02	0.15	<0.02	0.1	<0.02	0.08	<0.02
Tl	ICP-MS	0.02	0.19	0.17	0.3	0.28	0.15	0.3	0.21	0.18	0.69	0.59	0.16	0.07
Rb	ICP-MS	0.10	42.40	29.50	41.60	47.90	72.70	43.00	48.60	30.70	121.00	110.40	45.10	19.10
Sr	ICP-MS	0.50	987.00	1030.80	957.20	956.70	685.20	946.20	939.50	437.10	872.80	862.60	846.90	829.50
Nb	ICP-MS	0.10	9.40	8.10	7.30	7.40	8.30	8.40	8.50	7.40	18.10	10.00	6.00	8.30
Cs	ICP-MS	0.10	0.50	0.20	0.50	1.00	0.70	0.50	0.70	0.70	2.90	2.70	0.90	0.40
Be	ICP-MS	0.10	0.30	0.20	0.10	0.20	0.40	0.30	0.30	0.50	0.70	0.50	0.10	0.20
Hf	ICP-MS	0.10	5.80	5.10	5.20	5.10	5.00	5.00	5.30	2.60	7.30	6.30	4.30	6.90
Y	ICP-MS	0.10	23.50	19.90	19.40	20.00	23.60	23.10	21.30	22.00	30.60	23.40	17.30	24.70
Ta	ICP-MS	0.10	0.30	0.30	0.30	0.30	0.30	0.30	0.20	0.30	0.90	0.50	0.20	0.30
Sc	ICP-MS	0.10	1.80	1.80	1.90	1.50	2.20	2.20	2.10	2.30	2.60	1.90	1.40	1.60
V	ICP-MS	8.00	174.00	169.00	158.00	156.00	183.00	201.00	191.00	147.00	189.00	172.00	119.00	197.00
Mo	ICP-MS	0.01	0.21	0.19	0.16	0.21	0.36	0.23	0.22	0.21	0.34	0.37	0.15	0.2
As	ICP-MS	0.1	0.6	0.1	0.7	0.9	0.7	0.4	0.1	0.6	0.4	0.6	2.1	0.6
Sb	ICP-MS	0.02	<0.02	<0.02	<0.02	<0.02	<0.02	<0.02	<0.02	0.02	0.04	0.03	<0.02	0.02
W	ICP-MS	0.1	<0.1	<0.1	<0.1	<0.1	<0.1	<0.1	<0.1	<0.1	<0.1	<0.1	<0.1	<0.1
Hg	ICP-MS	0.01	<0.01	<0.01	<0.01	<0.01	<0.01	<0.01	<0.01	<0.01	<0.01	<0.01	<0.01	<0.01
Te	ICP-MS	0.02	<0.02	<0.02	<0.02	<0.02</td								

Alteration proximal to the sharp-walled Cu-(Ni)-PGE vein footwall mineralization of the Podolsky deposit, Sudbury

Table 1 continued.

	LM-P-039B	LM-P-007	11AV-72	11AV-73	11AV-74	11AV-53	11AV-56	LM-P-026	LM-P-027	LM-P-031	LM-P-055A	LM-P-055B	LM-P-055C	LM-P-055D
Laboratory	ACME	ActLabs	GeoLabs	GeoLabs	GeoLabs	GeoLabs	GeoLabs	ActLabs	ActLabs	ActLabs	ActLabs	ActLabs	ActLabs	ActLabs
wt%														
SiO ₂	47.50	51.4	47.72	48.10	51.23	49.90	50.77	48.22	49.82	42.96	57.1	51.56	51.5	51.21
TiO ₂	0.87	0.883	1.55	1.54	0.89	1.43	1.14	1.128	1.058	1.463	0.829	1.199	1.219	1.209
Al ₂ O ₃	16.24	14.79	16.05	16.33	15.76	16.29	16.43	14.29	14.33	15.11	15.43	16.58	16.39	16.25
FeO ^T	10.75	7.10	12.09	11.91	8.80	10.31	9.11	9.96	8.32	13.60	6.12	7.36	7.39	7.47
FeO	10.395	6.7	11.691	11.511	8.505	9.963	8.802	9	7.3	11.6	5.3	6.6	6.5	6.6
Fe ₂ O ₃	1.16	1.29	1.30	1.28	0.95	1.11	0.98	3.08	3.29	6.44	2.63	2.46	2.86	2.81
MgO	5.13	7.57	5.04	5.12	6.83	4.86	5.71	6.5	6.41	5.75	3.46	5.26	5.25	5.49
MnO	0.13	0.145	0.15	0.15	0.14	0.16	0.13	0.134	0.172	0.179	0.084	0.13	0.136	0.135
CaO	10.10	8.51	8.36	8.42	7.94	7.15	7.73	5.05	7.56	3.8	4.51	7.42	7.64	7.94
Na ₂ O	3.56	3.22	3.31	3.33	3.00	3.38	3.55	2.38	3.26	2.11	3.55	3.57	3.63	3.51
K ₂ O	0.28	1.41	2.04	2.05	2.11	2.34	1.90	1.07	0.59	0.07	1.77	1.97	1.94	1.96
P ₂ O ₅	0.84	0.48	1.17	1.16	0.65	0.76	0.61	0.54	0.53	0.7	0.45	0.66	0.73	0.68
LOI	2.53	0.98	1.15	1.15	1.56	1.78	0.99	4.3	3.31	5.97	1.86	1.49	1.64	1.49
Total	96.79	98.91	98.35	98.97	97.97	97.29	96.7	98.44	97.47	97.59	99.63	100.2	100	
TOT/C	<0.02	0.06	0.16	0.12	0.08	0.28	0.14	0.03	0.09	0.07	0.04	0.03	0.06	0.03
FeO	5.96	7.4						9	7.3	11.6	5.3	6.6	6.5	6.6
TOT/S	0.54	0.23	0.27	0.26	0.19	0.16	0.19	1.22	0.34	0.61	0.27	0.16	0.19	0.19
Cl	0.04							0.11	0.05	0.08	0.11	0.07	0.07	0.08
F	0.06							0.06	0.06	0.05	0.07	0.07	0.07	0.08
ppm														
B	1	<1						1	<1	<1	<1	8	7	17
Li	13.4	22	16.7	17.1	18.9	19.3	14.3	46	32	28	25	24	22	22
ppb														
Se	300.00	<2	73.30	71.10	95.00	229.50	136.40	94	160	17100	327	2	<2	<2
Au	6.20	1	2.00	2.00	2.00	4.00	2.30	109	237	2330	818	2	<1	<1
Pd	<10	<1						401	58	119	194	<1	<1	<1
Pt	<2													
Ag	383	2300	120	130	250	710	590	3700	5500	15700	3300	2500	2700	2700
Re	<1													
ppm														
Cu	5616.60	50	43.00	47.00	67.00	1389.00	105.00	7250	2550	5330	2010	1100	910	110
Ni	49.30	120	46.00	45.00	100.00	66.00	69.00	9260	2590	6400	250	60	70	60
Co	29.70	68	39.61	39.92	40.94	33.57	35.48	82.9	54	57.1	49.1	40.3	37.3	43.5
Cr	47.10	220	56.00	57.00	166.00	58.00	121.00	170	130	60	60	90	90	100
Mn	412	1130	1037	1027	1022	1065	901	982	1390	1330	649	983	1010	991
Zn	90.00	125	183.00	167.00	140.00	219.00	125.00	256	261	261	171	167	166	171
Sn	2	<1	1.56	1.55	1.17	1.72	1.48	17	21	18	7	2	1	1
Ga	21.5	18	20.9	21.29	17.79	20.23	19.83	15	17	21	19	20	20	20
Ge	0.1	1.7						1.3	1.7	1.3	1.3	1.3	1.3	1.2
In	<0.02	<0.2	0.004	0.003	0.003	0.006	0.013	1	0.9	0.6	<0.2	<0.2	<0.2	<0.2
Cd	0.09	<0.2	0.252	0.152	0.358	0.151	0.923	1.2	0.2	0.3	<0.2	0.4	0.5	0.6
La	98.30	65	93.83	94.46	73.21	92.12	85.96	62.5	58.7	72.1	75.3	73.6	76.3	70.7
Ce	198.20	137	197.29	195.09	148.35	188.58	170.73	137	127	154	150	156	164	152
Pr	23.39	15.6	23.49	23.13	17.59	22.31	19.86	15.3	14.6	17.5	16.1	18	19	17.7
Nd	88.90	59.6	87.94	88.08	65.69	84.88	74.22	57.5	55.4	65.8	58.5	68	72	68.1
Sm	13.62	9.85	13.87	13.98	10.29	13.57	11.59	8.88	9.44	10.3	9.28	11.3	12	11.4
Eu	3.56	2.27	3.22	3.32	2.45	3.32	2.87	1.61	1.69	1.85	2.12	2.61	2.69	2.65
Gd	9.70	6.5	9.13	9.26	6.80	9.04	7.65	5.7	6.08	6.67	6.02	7.17	7.19	7.36
Tb	1.04	0.8	1.06	1.07	0.81	1.07	0.93	0.66	0.72	0.83	0.74	0.88	0.9	0.93
Dy	5.12	3.84	5.32	5.43	4.16	5.34	4.61	3.33	3.6	3.99	3.68	4.33	4.36	4.65
Ho	0.86	0.68	0.93	0.93	0.72	0.94	0.81	0.58	0.63	0.72	0.64	0.74	0.77	0.83
Er	2.42	1.82	2.39	2.34	1.94	2.43	2.13	1.65	1.73	1.99	1.73	1.99	2.11	2.24
Tm	0.33	0.261	0.30	0.30	0.25	0.31	0.28	0.243	0.243	0.279	0.237	0.281	0.29	0.311
Yb	2.00	1.63	1.87	1.83	1.57	1.87	1.72	1.54	1.54	1.78	1.5	1.76	1.87	1.91
Lu	0.27	0.242	0.26	0.26	0.23	0.26	0.24	0.237	0.236	0.28	0.251	0.264	0.292	0.292
Zr	329.30	208	218.00	193.00	157.00	105.00	220.00	296	217	258	245	237	243	244
Ba	154.00	940	1172.70	1117.80	1000.30	>1740	1257.20	546	423	58	902	1189	1217	1151
Pb	16.40	15	12.40	12.40	26.60	18.50	69.40	36	13	19	138	39	31	27
Th	3.50	2.23	2.00	2.21	2.44	2.47	3.73	7.7	1.76	3.01	13.3	2.76	1.8	1.49
U	0.20	0.21	0.31	0.32	0.25	0.14	0.13	0.55	0.19	0.41	4.52	0.45	0.13	0.12
Bi	<0.02	<0.1	0.01	0.01	0.08	0.09	1.26	16.1	8.5	3.2	1.6	0.3	0.3	0.2
Tl	0.05	0.38	0.38	0.375	0.412	0.251	0.295	0.41	0.15	0.06	0.74	0.53	0.39	0.38
Rb	8.10	39	59.99	59.92	61.84	62.79	47.40	35	15	2	73	54	48	51
Sr	1341.80	882	956.40	980.60	839.00	901.10	988.00	679	872	328	748	974	1012	1006
Nb	10.20	7.1	9.78	9.54	7.52	10.25	8.72	10.7	7.3	9.3	10.7	9.5	9.5	8.7
Cs	0.30	0.5	1.27	1.36	1.31	0.73	0.44	0.8	0.3	<0.1	1.4	0.8	0.6	0.6
Be	0.30	2	1.37	1.37	1.19	1.49	1.47	<1	1	<1	2	2	2	2
Hf	7.10	4.6	4.67	4.18	3.66	2.51	4.74	6.4	4.9	5.7	5.7	5.3	5.4	5.6
Y	26.10	18.5	25.11	24.95	19.06	24.51	21.87	15.5	16.7	19.9	17.4	20.7	21.3	21.4
Ta	0.30	1.71	0.37	0.37	0.24	0.33	0.26	1.17	1.01	1.18	1.68	0.88	0.87	0.73
Sc	2.50	23	21.30	21.10	20.10	19.90	20.30	16	19	17	13	18	18	19
V	217.00	147	238.30	235.60	131.00	183.90	154.80	136	147	206	118	174	178	175
Mo	0.41	<5	0.65	0.73	0.33	0.48	0.32	<1	<1	<1	1	<1	<1	<1
As	1	<1	0.9	1	2.5			6	<5	<5	<5	<5	<5	<5
Sb	0.09	<0.2			0.08	0.11		<0.2	<0.2	<0.2	<0.2	<0.2	<0.2	<0.2
W	<0.1		0.42	0.92	0.05									
Hg	<0.01		0.01	0.01		0.01	0.01							
Te	0.04		10	10	10									
Mg#	30.8	49.9	28.0	28.6	42.0	30.5	36.9	39.5	43.5	29.7	36.1	41.7	41.5	42.4
⁸⁷ Sr/ ⁸⁶ Sr			0.70342					7.2	6.3	6.3	8.2	6.7	7.2	6.5

Table 1 continued.

	LM-P-060A	LM-P-060B	Actinolite Crystals	LM-P-043A	LM-P-043B	LM-P-043C	LM-P-043D	LM-P-043E	LM-P-043F	LM-P-043G	LM-P-043H-1	LM-P-043H-2	LM-P-043I	LM-P-043J
Laboratory	ActLabs	ActLabs		ACME	ACME	ACME	ACME	ACME	ActLabs	ActLabs	ActLabs	ActLabs	ActLabs	ActLabs
wt%														
SiO ₂	52.34	51.15		51.5	51.6	51.3	53.5	51.5	50.97	50.99	50.97	51.7	51.13	50.87
TiO ₂	0.799	0.822		0.82	0.82	0.84	0.68	0.81	0.839	0.819	0.798	0.819	0.818	0.825
Al ₂ O ₃	14.08	15.26		15.56	15.84	15.69	15.92	15.63	15.54	15.82	15.69	15.87	15.5	15.5
FeOT	9.66	8.73		10.11	9.24	9.24	8.54	9.04	7.61	7.68	7.46	7.39	7.44	7.38
FeO	8.8	8.1		9.77	8.93	8.94	8.25	8.74	7.3	7.5	7.1	6.9	7.1	7
Fe ₂ O ₃	2.77	2.03		1.09	0.99	0.96	0.92	0.97	1.01	0.58	1.17	1.58	1.1	1.21
MgO	6.93	6.45		6.99	7.19	7.27	5.92	7.21	7.08	6.82	6.57	6.79	6.81	6.87
MnO	0.153	0.147		0.16	0.15	0.15	0.27	0.15	0.147	0.145	0.148	0.15	0.146	0.143
CaO	5.3	6.41		6.86	7.35	7.57	7.07	7.55	8	8.02	7.83	8	7.92	8.01
Na ₂ O	3.73	3.97		3.26	3.37	3.39	2.79	3.3	3.16	3.2	3.17	3.16	3.25	3.2
K ₂ O	0.54	0.73		1.55	1.77	1.91	1.02	1.77	1.85	1.86	1.67	1.76	1.89	1.9
P ₂ O ₅	0.37	0.4		0.38	0.39	0.4	0.19	0.38	0.4	0.4	0.37	0.38	0.38	0.39
LOI	2.93	2.77		1.81	1.67	1.6	2.42	1.65	1.65	1.63	1.76	1.77	1.8	1.68
Total	99.73	99.14		99.83	100.18	99.85	98.99	99.74	98.77	98.62	98.04	99.66	98.63	98.39
TOT/C	0.01	0.04		0.03	0.11	0.04	0.2	0.05	0.07	0.05	0.06	0.06	0.07	0.05
FeO	8.8	8.1		8.64	7.67	7.51	6.53	7.59	7.3	7.5	7.1	6.9	7.1	7
TOT/S	0.42	0.08		0.23	0.13	0.15	0.09	0.2	0.17	0.16	0.21	0.19	0.16	0.19
Cl	0.08	0.08							0.09	0.09	0.08	0.09	0.09	0.1
F	0.07	0.07							0.07	0.07	0.06	0.06	0.07	0.06
ppm														
B	7	8												
Li	19	23		20.5	21.8	23.5	11.8	24.1	17	26	12	10	9	<1
ppb														
Se														
Au	168	39		166.4	41.2	12.9	5.1	14.8	2	<2	4	4	<2	<2
Pd	107	4		135	16	<10	<10	25	2	1	6	8	<1	<1
Pt	343	20		230	274	55	<2	22	<1	<1	15	18	<1	<1
Ag	2200	2800		2110	1391	1187	239	1138	4800	3700	3400	3200	3200	2800
Re														
ppm														
Cu	2790	920		2099.69	902.49	653.19	248.27	1496.36	170	550	1570	1520	510	100
Ni	3530	1670		199.8	121	135	70.2	672.4	100	90	150	150	90	100
Co	42.3	45		34.3	32.5	35.7	20	32.1	45.5	44.9	38.5	37.3	45.6	45
Cr	190	210		110	109.2	106.9	73.1	99	170	170	160	160	170	170
Mn	1090	1130		399	341	333	591	371	1150	1120	1130	1180	1190	1070
Zn	241	235		111	239	653	63	112	245	255	157	157	337	203
Sn	15	6		4	2	1	2	2	<1	<1	2	2	<1	<1
Ga	15	17		17.5	16.7	17.6	15.6	17.6	18	18	18	18	18	18
Ge	1.2	1.8		0.1	0.1	<0.1	<0.1	<0.1	1.6	1.5	1.5	1.7	1.5	1.5
In	0.6	0.3		0.03	0.02	0.02	0.04	<0.02	<0.2	<0.2	<0.2	<0.2	<0.2	<0.2
Cd	0.6	0.8		1.3	7.58	25.9	1.17	1.96	4.5	4.6	0.9	1	6.7	3.2
La	45.3	57.4		64.1	65.7	68.8	18	65	62	62.5	60.8	61.1	63.3	62.4
Ce	98.8	117		124	128.1	135.1	35.9	129	128	128	122	124	127	128
Pr	11.4	14		14.84	14.93	15.54	4.48	15.3	14.3	14.2	13.6	13.9	14.3	14.2
Nd	43.7	49.2		57.6	55.2	58.1	18.4	56	53.4	53.8	51	52.4	53.1	53.5
Sm	7.58	8.04		8.68	8.4	9.03	3.46	9.02	8.81	9.08	8.65	8.39	8.89	8.63
Eu	1.34	1.7		2.23	2.1	2.14	0.99	2.15	2.11	2.08	2.05	2.08	2.11	2.12
Gd	4.77	5.98		6.3	5.89	6.53	3.2	6.22	5.87	5.86	5.37	5.39	5.65	5.68
Tb	0.62	0.69		0.69	0.66	0.7	0.4	0.71	0.69	0.69	0.68	0.68	0.7	0.72
Dy	3	3.49		3.67	3.43	3.79	2.46	3.81	3.5	3.55	3.4	3.37	3.43	3.37
Ho	0.51	0.58		0.6	0.57	0.59	0.46	0.63	0.63	0.64	0.58	0.6	0.62	0.59
Er	1.4	1.6		1.7	1.59	1.77	1.46	1.76	1.7	1.71	1.59	1.65	1.66	1.57
Tm	0.196	0.228		0.22	0.22	0.22	0.2	0.23	0.237	0.235	0.219	0.23	0.225	0.22
Yb	1.26	1.41		1.44	1.39	1.46	1.32	1.56	1.44	1.48	1.44	1.5	1.49	1.44
Lu	0.201	0.208		0.21	0.18	0.21	0.18	0.22	0.218	0.222	0.227	0.239	0.231	0.232
Zr	171	205		186.4	230.4	265.6	85.8	220.5	214	209	213	205	213	217
Ba	381	585		960	958	1053	423	897	961	952	1002	1041	994	994
Pb	34	42		29.3	52.3	69.9	9.6	31.8	108	122	40	49	124	120
Th	3.8	2.33		3.2	3.2	3.2	2.2	4.2	2.78	2.83	3.12	3.06	2.85	2.84
U	0.32	0.19		0.4	0.1	0.3	0.9	0.9	0.15	0.14	0.5	0.47	0.15	0.15
Bi	2.1	2.8		1.33	1.71	1.04	0.32	0.57	0.6	1	0.6	0.8	0.9	0.3
Tl	0.2	0.16		0.49	0.33	0.35	0.13	0.39	0.48	0.55	0.58	0.54	0.53	0.52
Rb	16	20		43.1	50.1	60.7	30.4	56.1	56	57	54	55	60	60
Sr	515	746		765.1	805.4	854.4	438	835.1	892	910	915	899	891	899
Nb	6.3	7.1		6.5	6.8	7.2	3.5	8	6.7	6.6	6.7	6.8	6.7	6.7
Cs	0.4	0.5		0.8	0.7	0.8	2.9	0.9	0.6	0.7	0.8	0.8	0.8	0.8
Be	1	2		0.2	0.2	0.2	0.2	0.2	1	2	2	2	2	2
Hf	3.9	4.6		4.1	5.4	5.9	2.6	5	4.7	4.5	4.8	4.3	4.7	4.8
Y	13.9	15.8		17.7	17.3	18.8	13.3	19.3	16.7	16.4	15.5	16.4	16.2	16.1
Ta	0.53	0.75		0.2	0.2	0.3	0.2	0.3	0.58	0.71	0.85	0.7	0.65	0.68
Sc	22	22		1.6	1.4	1.5	4.4	1.9	20	20	19	20	20	20
V	123	139		126	118	130	191	121	133	133	129	132	134	132
Mo	<1	<1		0.4	0.2	0.2	0.8	0.5	<1	2	<1	<1	<1	<1
As	<5	<5		0.3	0.2	<0.1	1.1	0.3	<5	<5	<5	<5	<5	<5
Sb	<0.2	<0.2		<0.02	<0.02	<0.02	0.14	<0.02	<0.2	<0.2	<0.2	<0.2	<0.2	<0.2
W				<0.1	<0.1	<0.1	0.1	<0.1						
Hg				<0.01	<0.01	0.01	<0.01	0.01						
Te				0.33	0.17	0.06	0.07	0.13						
Mg#	41.8	42.5		40.9	43.8	44.0	41.0	44.4	48.2	47.0	46.8	47.9	47.8	48.2
δ ¹⁸ O	6.4	7.3	5.0	6.7		7.1		12.7		6.6		0.703050		
⁸⁷ Sr/ ⁸⁶ Sr														

Alteration proximal to the sharp-walled Cu-(Ni)-PGE vein footwall mineralization of the Podolsky deposit, Sudbury

Table 1 continued.

	LM-P-043K	LM-P-043L-1	LM-P-043L-2	LM-P-043M	LM-P-043N	LM-P-043O-1	LM-P-043O-2	LM-P-043P
Laboratory	ActLabs	ActLabs	ActLabs	ActLabs	ActLabs	ActLabs	ActLabs	ActLabs
wt%								
SiO ₂	51.29	51.01	50.91	50.57	51.41	51.17	51.24	51.82
TiO ₂	0.837	0.79	0.815	0.821	0.793	0.82	0.804	0.81
Al ₂ O ₃	15.35	15.54	15.25	15.88	15.45	15.8	15.94	15.74
FeO ^T	7.23	7.17	7.37	7.38	7.48	7.74	7.13	7.23
FeO	6.8	6.8	7	6.9	6.9	7.6	6.7	6.7
Fe ₂ O ₃	1.39	1.19	1.18	1.54	1.88	0.46	1.37	1.72
MgO	7.05	6.78	6.97	6.71	6.74	6.84	6.8	6.81
MnO	0.143	0.142	0.143	0.148	0.142	0.139	0.138	0.142
CaO	7.93	7.97	7.86	7.75	7.76	7.79	7.98	7.74
Na ₂ O	3.19	3.22	3.19	3.05	3.11	3.28	3.2	3.22
K ₂ O	1.92	1.81	1.84	1.81	1.69	1.82	2.01	1.83
P ₂ O ₅	0.4	0.4	0.39	0.39	0.39	0.38	0.35	0.38
LOI	1.87	1.66	1.83	1.9	2	1.84	1.56	2.05
Total	98.94	98.07	98.16	98.25	99.05	98.79	98.85	99.73
TOT/C	0.06	0.06	0.05	0.04	0.05	0.05	0.07	0.08
FeO	6.8	6.8	7	6.9	6.9	7.6	6.7	6.7
TOT/S	0.18	0.17	0.16	0.18	0.32	0.14	0.18	0.18
Cl	0.08	0.08	0.11	0.07	0.08	0.1	0.1	0.1
F	0.07	0.07	0.07	0.07	0.06	0.06	0.07	0.06
ppm								
B	6	10	11	12	14	17	14	12
Li	23	23	27	27	27	31	25	32
ppb								
Se								
Au	<2	2	<2	6	18	2	<2	53
Pd	<1	<1	<1	7	137	<1	<1	41
Pt	3	<1	<1	48	201	<1	<1	33
Ag	2400	3200	2800	2700	2700	2600	2600	2400
Re								
ppm								
Cu	210	1230	790	1500	1980	870	130	1220
Ni	100	100	100	250	510	140	90	360
Co	47	43.1	46.2	47.1	43.5	44.5	54.3	51.1
Cr	170	160	180	160	160	160	160	160
Mn	1040	1120	1140	1160	1130	1160	1090	1190
Zn	244	163	212	157	176	242	349	296
Sn	<1	<1	<1	2	4	<1	<1	1
Ga	18	18	18	18	18	18	18	18
Ge	1.4	1.5	1.4	1.3	1.5	1.5	1.5	1.4
In	<0.2	<0.2	<0.2	<0.2	<0.2	<0.2	<0.2	<0.2
Cd	5	1.3	3.3	0.5	1	3.9	7.7	4.7
La	59.9	61.5	60.8	60.9	61.3	62.3	59.9	60.4
Ce	124	125	124	124	121	125	120	122
Pr	14.2	14	14.3	13.8	13.5	14	13.5	13.4
Nd	52.4	52.2	53.3	52.1	51.4	52.5	50.8	50.1
Sm	8.81	8.81	9.32	8.81	8.54	8.8	8.21	8.27
Eu	2.08	2.13	2.04	2.11	2.1	2.09	2.1	2.01
Gd	5.77	5.56	5.63	5.6	5.71	5.62	5.47	5.42
Tb	0.75	0.75	0.75	0.68	0.77	0.67	0.7	0.71
Dy	3.84	3.78	3.82	3.52	3.87	3.45	3.47	3.63
Ho	0.69	0.69	0.67	0.62	0.68	0.62	0.6	0.63
Er	1.89	1.87	1.8	1.68	1.88	1.73	1.61	1.7
Tm	0.266	0.259	0.258	0.24	0.27	0.246	0.223	0.24
Yb	1.7	1.68	1.7	1.54	1.68	1.51	1.39	1.5
Lu	0.27	0.266	0.274	0.242	0.256	0.228	0.223	0.238
Zr	189	203	215	196	199	215	203	206
Ba	985	930	942	1040	922	944	966	953
Pb	124	44	75	36	70	55	90	49
Th	4.06	3.46	3.31	3.17	3.71	2.77	2.71	3.17
U	1.36	0.92	0.9	0.53	1.15	0.15	0.15	0.5
Bi	0.4	0.4	0.6	0.6	1	0.6	0.6	0.6
Tl	0.53	0.57	0.52	0.59	0.59	0.54	0.58	0.53
Rb	63	60	61	62	59	58	63	58
Sr	880	922	871	897	884	919	918	894
Nb	7.9	7.5	7.8	7.1	7.7	6.7	6.6	6.9
Cs	1.1	1.1	1.1	1.1	1	0.7	0.8	0.8
Be	2	2	2	2	2	2	2	2
Hf	4.2	4.5	5	4.5	4.5	4.6	4.4	4.7
Y	19.1	17.9	18.7	16.5	18.3	16.1	15.9	16.1
Ta	0.99	0.83	1.56	0.92	0.9	0.75	0.94	1.03
Sc	20	20	20	19	20	20	20	19
V	134	128	130	129	128	128	128	129
Mo	<1	<1	<1	<1	<1	2	<1	<1
As	<5	<5	<5	<5	<5	<5	<5	<5
Sb	<0.2	<0.2	<0.2	<0.2	<0.2	<0.2	<0.2	<0.2
W								
Hg								
Te								
Mg#	49.4	48.6	48.6	47.6	47.4	46.9	48.8	48.5
$\delta^{18}\text{O}$	8.0							7.1
$^{87}\text{Sr}/^{86}\text{Sr}$								

Table 2. Petrography and modal mineralogy of the chalcopyrite-rich ore, altered grey gabbro, and less altered grey gabbro of the Podolsky deposit.

LOCATION	Sample #	Plag	Augite	OPX	Hornblende	Pseudo Actinolite	Pseudo Red- Brown Biotite	Biotite	Pseudo Chlorite	Quartz	Epidote	Apatite	Metamorphic/ Magmatic Zircons
UNKNOWN	LM-P-007	45	10	TR	8	5	15	5	-	TR	TR	5	TR
FNX4307-660ft	LM-P-025	50	5	TR	10	15	15	TR	-	TR	TR	4	TR
FNX4307-615ft	LM-P-021	50	3	TR	8	12	20	1	TR	TR	TR	4	TR
FNX4307-400ft	LM-P-019	47	7	TR	8	10	15	1	2	TR	TR	3	TR
FNX4306-532ft	LM-P-032A	47	4	TR	7	15	12	3	3	TR	TR	5	TR
1700 Haulage	LM-P-042	47	3	TR	8	20	15	1	TR	TR	TR	3	TR
FNX4306-545ft	LM-P-033	49	2	TR	5	16	10	3	5	TR	TR	7	TR
FNX4306-825ft	LM-P-028	48	TR	TR	3	20	15	1	5	TR	TR	4	TR
UNKN	LM-P-008	47	TR	TR	8	20	7	TR	5	1	TR	5	TR
FNX4306-845ft	LM-P-038	44	-	TR	TR	20	16	TR	8	TR	TR	4	TR
FNX4306-830ft	LM-P-039A	37	TR	TR	10	15	1	TR	12	2	TR	2	TR
	LM-P-039B	20	-	TR	TR	3	4	TR	8	TR	TR	1	5
FNX4306-500ft	LM-P-030	36	-	TR	TR	17	10	TR	5	-	TR	7	3
FNX4306-855ft	LM-P-037	15	TR	TR	TR	15	5	2	10	-	TR	7	TR
FNX4306-865ft	LM-P-036	-	TR	TR	TR	5	TR	-	TR	-	TR	1	TR
2225L-9450 Drift	LM-P-043A	45	3	TR	2	18	10	5	TR	TR	TR	2	TR
	LM-P-043B	45	4	1	3	20	15	5	1	TR	TR	2	TR
	LM-P-043C	45	8	1	3	20	10	5	1	1	TR	2	TR
	LM-P-043D	45	6	TR	4	20	10	5	1	TR	TR	3	TR
	LM-P-043E	45	2	TR	1	23	15	7	2	TR	TR	3	TR
	LM-P-043F	45	3	TR	1	20	20	5	2	TR	TR	3	TR
	LM-P-043G	45	5	TR	3	22	15	5	TR	TR	TR	3	TR
	LM-P-043H	50	3	TR	2	22	12	5	1	TR	TR	2	TR
	LM-P-043I	45	4	TR	1	20	15	7	2	1	TR	3	TR
	LM-P-043J	45	6	TR	3	18	15	4	1	1	TR	3	TR
	LM-P-043K	40	3	TR	1	25	15	7	2	1	TR	3	TR
	LM-P-043L	40	6	TR	1	25	15	5	1	TR	TR	2	TR
	LM-P-043M	40	5	TR	3	20	20	5	1	TR	TR	2	TR
	LM-P-043N	45	4	TR	1	15	22	8	1	TR	TR	2	TR
	LM-P-043O	45	8	TR	3	23	10	6	1	TR	TR	2	TR
	LM-P-043P	45	8	TR	2	26	10	5	TR	TR	TR	2	TR
	LM-P-043Q	45	6	TR	1	25	8	5	TR	TR	TR	3	TR
1925L-Haulage	LM-P-044A	40	6	TR	3	28	10	5	TR	TR	TR	2	TR
	LM-P-044B	45	7	TR	1	25	10	6	TR	TR	TR	3	TR
	LM-P-044C	45	10	TR	5	25	7	4	TR	TR	TR	2	TR
	LM-P-044D	45	7	TR	2	25	10	5	TR	TR	TR	3	TR
	LM-P-044E	45	10	TR	5	20	10	4	TR	TR	TR	3	TR
	LM-P-044F	40	10	TR	5	30	7	3	TR	TR	TR	2	TR
	LM-P-044G	45	10	TR	3	28	8	2	TR	TR	TR	2	TR
	LM-P-044H	45	10	TR	3	20	10	6	TR	TR	TR	2	TR
1700L-450RMK	LM-P-045A	40	4	TR	TR	30	10	4	2	1	TR	2	TR
	LM-P-045B	45	3	TR	1	26	7	8	TR	TR	TR	2	TR
	LM-P-045C	45	4	TR	2	30	10	5	TR	TR	TR	2	TR
	LM-P-045D	45	2	TR	2	30	10	5	2	TR	TR	2	TR
	LM-P-045E	45	8	TR	1	28	10	5	TR	TR	TR	1	TR
DDH4938	LM-P-055A												
	LM-P-055B	15	TR	TR	TR	20	5	15	TR	TR	TR	2	TR
	LM-P-055C	40	4	TR	2	30	5	2	TR	1	TR	2	TR
	LM-P-055D	40	3	TR	TR	30	15	5	TR	1	TR	2	TR
	LM-P-055E	40	4	TR	1	25	18	5	TR	1	TR	2	TR
	LM-P-055F	40	6	TR	2	25	15	5	TR	TR	TR	2	TR
	LM-P-055G	40	6	TR	2	25	15	5	TR	TR	TR	3	TR
	LM-P-055H	45	6	TR	3	22	10	5	TR	TR	TR	3	TR
	LM-P-055I	50	4	TR	TR	20	15	5	TR	TR	TR	2	TR
1700-RMK	LM-P-060A												
	LM-P-060B	25	8	TR	1	15	TR	3	1	TR	TR	2	TR
	LM-P-060C	40	6	TR	1	30	8	3	TR	TR	TR	1	TR
	LM-P-060D	40	8	TR	1	30	7	2	TR	TR	TR	1	TR
	LM-P-060E	40	3	TR	2	35	1	2	TR	TR	TR	1	TR
	LM-P-060F	40	6	TR	2	35	3	4	TR	TR	TR	1	TR

Note: Plag = plagioclase; OPX = orthopyroxene; TR = trace.

Table 2 continued.

LOCATION	Sample #	Total % of disseminated sulphide	Chalcopyrite	Ilmenite	Pyrite	Magnetite	Total % of veins/clots	Quartz	Chlorite	Epidote	Plagioclase	Biotite
UNKNOWN	LM-P-007	1	TR	TR	TR	1	6	TR	TR	3	2	1
FNX4307-660ft	LM-P-025	1	TR	TR	TR	1	TR	TR	-	TR	-	TR
FNX4307-615ft	LM-P-021	2	TR	TR	TR	2	TR	TR	-	TR	-	-
FNX4307-400ft	LM-P-019	1	TR	TR	TR	1	6	TR	3	3	-	-
FNX4306-532ft	LM-P-032A	1	TR	TR	TR	1	3	TR	TR	3	-	-
1700 Haulage	LM-P-042	TR	TR	TR	TR	TR	3	TR	TR	3	-	-
FNX4306-545ft	LM-P-033	2	TR	TR	TR	2	1	TR	TR	1	TR	-
FNX4306-825ft	LM-P-028	2	TR	TR	TR	2	2	TR	TR	2	-	-
UNKN	LM-P-008	3	1	TR	TR	2	4	TR	1	3	TR	-
FNX4306-845ft	LM-P-038	1	TR	TR	TR	1	7	2	1	3	1	TR
FNX4306-830ft	LM-P-039A	1	1	TR	-	TR	20	7	7	6	TR	-
	LM-P-039B	3	1	TR	TR	2	56	4	16	6	20	TR
FNX4306-500ft	LM-P-030	2	TR	TR	TR	2	18	2	4	5	2	-
FNX4306-855ft	LM-P-037	1	TR	TR	TR	1	45	5	10	15	15	TR
FNX4306-865ft	LM-P-036	2	1	TR	TR	1	92	5	25	10	45	5
	LM-P-043A	1	0.5	0.1	0.1	0.5	10	3	0	-	-	-
	LM-P-043B	1	1	0.1	0.1	0.5	3	-	3	-	-	-
	LM-P-043C	1	0.5	0.5	0.1	0.1	3	-	3	-	-	-
	LM-P-043D	1	0.5	0.5	0.1	0.1	5	3	2	TR	TR	-
	LM-P-043E	1	0.5	0.1	0.1	0.1	1	1	TR	TR	-	-
	LM-P-043F	1	0.5	0.5	0.5	0.1	0	-	-	TR	TR	-
	LM-P-043G	1	0.5	0.5	0.1	0.1	1	1	TR	-	-	-
	LM-P-043H	1	0.5	0.1	0.5	0.1	2	-	2	-	-	-
2225L-9450 Drift	LM-P-043I	1	0.5	0.5	0.5	0.1	1	-	1	-	-	-
	LM-P-043J	1	0.5	0.5	0.1	0.1	3	2	1	-	-	-
	LM-P-043K	1	0.5	0.5	0.1	0.1	2	1	1	-	-	-
	LM-P-043L	2	2	0.5	0.1	0.1	3	1	2	TR	-	-
	LM-P-043M	1	0.5	0.5	0.1	0.1	3	1	2	TR	-	-
	LM-P-043N	1	0.5	0.5	0.1	0.1	1	-	1	-	-	-
	LM-P-043O	TR	0.1	0.1	0.5	0.1	2	TR	2	-	-	-
	LM-P-043P	1	0.2	1	0.1	0.1	1	-	1	-	-	-
	LM-P-043Q	1	1	0.5	0.1	0.1	6	3	3	-	-	-
	LM-P-044A	1	1	0.1	0.1	0.1	2	1	1	-	-	-
	LM-P-044B	2	1	1	0.1	0.1	1	TR	1	-	-	-
	LM-P-044C	1	0.5	0.1	0.1	1	1	0.5	0.5	-	-	-
1925L-Haulage	LM-P-044D	2	1	1	0.1	0.1	1	0.5	0.5	-	-	-
	LM-P-044E	1	0.5	1	0.5	0.1	2	1	1	-	-	-
	LM-P-044F	2	0.5	2	0.5	0.1	1	0.5	0.5	-	-	-
	LM-P-044G	1	0.5	1	0.1	0.1	1	0.5	1	-	-	-
	LM-P-044H	2	0.5	2	0.1	0.1	2	1	1	-	TR	TR
	LM-P-045A	2	2	0.5	0.1	0.1	5	1	3	-	1	TR
1700L-450RMK	LM-P-045B	1	0.5	1	0.1	0.1	7	2	2	-	-	3
	LM-P-045C	1	0.5	1	0.1	0.1	1	TR	1	-	-	-
	LM-P-045D	1	1	0.5	0.1	0.1	1	-	1	-	-	-
	LM-P-045E	1	0.5	0.5	0.5	0.1	1	-	1	-	-	-
	LM-P-055A							-	-	-	-	-
	LM-P-055B	5	2	0.1	0.1	3	10	8	1	-	1	-
	LM-P-055C	2	0.5	1	0.1	1	12	7	5	-	-	-
	LM-P-055D	2	1	0.5	0.1	0.5	2	1	1	-	-	-
DDH4938	LM-P-055E	1	0.5	0.1	0.1	1	3	2	1	-	-	-
	LM-P-055F	2	0.5	1	0.1	1	3	1	2	-	-	-
	LM-P-055G	2	1	1	0.5	0.5	2	1	1	-	-	-
	LM-P-055H	1	0.1	1	0.5	0.5	5	TR	5	-	-	-
	LM-P-055I	2	1	0.5	0.1	0.5	2	1	1	-	-	-
	LM-P-060A							-	-	-	-	-
	LM-P-060B	5	5	0.1	0.1	0.5	20	2	2	1	-	-
1700-RMK	LM-P-060C	1	1	0.1	0.1	0.1	10	3	3	TR	4	TR
	LM-P-060D	1	1	0.1	0.1	0.1	10	1	8	-	TR	-
	LM-P-060E	1	0.5	0.5	0.1	0.5	15	3	10	-	-	2
	LM-P-060F	TR	0.5	0.5	0.1	0.1	9	1	8	-	-	-

Note: TR = trace.

Table 2 continued.

LOCATION	Sample #	Actinolite Calcite	% dust cluster hosted by plagioclase	% of corona surrounding mafic minerals	Total % of massive sulphide	Chalcopyrite	Ilmenite	Magnetite	Bornite	Pyrite	Gangue
UNKNOWN	LM-P-007	- -	25	10	-	- - -	- - -	- - -	- - -	- - -	- - -
FNX4307-660ft	LM-P-025	- -	10	30	-	- - -	- - -	- - -	- - -	- - -	- - -
FNX4307-615ft	LM-P-021	- -	10	30	-	- - -	- - -	- - -	- - -	- - -	- - -
FNX4307-400ft	LM-P-019	- -	25	20	-	- - -	- - -	- - -	- - -	- - -	- - -
FNX4306-532ft	LM-P-032A	- -	20	20	-	- - -	- - -	- - -	- - -	- - -	- - -
1700 Haulage	LM-P-042	- -	20	25	-	- - -	- - -	- - -	- - -	- - -	- - -
FNX4306-545ft	LM-P-033	- -	15	20	-	- - -	- - -	- - -	- - -	- - -	- - -
FNX4306-825ft	LM-P-028	- -	20	25	-	- - -	- - -	- - -	- - -	- - -	- - -
UNKN	LM-P-008	- -	25	40	-	- - -	- - -	- - -	- - -	- - -	- - -
FNX4306-845ft	LM-P-038	- -	35	30	-	- - -	- - -	- - -	- - -	- - -	- - -
FNX4306-830ft	LM-P-039A	- TR	40	40	-	- - -	- - -	- - -	- - -	- - -	- - -
	LM-P-039B	10 TR	50	35	-	- - -	- - -	- - -	- - -	- - -	- - -
FNX4306-500ft	LM-P-030	- 5	45	30	-	- - -	- - -	- - -	- - -	- - -	- - -
FNX4306-855ft	LM-P-037	- TR	45	35	-	- - -	- - -	- - -	- - -	- - -	- - -
FNX4306-865ft	LM-P-036	2 TR	50	50	-	- - -	- - -	- - -	- - -	- - -	- - -
2225L-9450 Drift	LM-P-043A	7 -	35	20	4	3 0	1 0	0 -	- 1	- -	- -
	LM-P-043B	- -	20	30	0	- - -	- - -	- - -	- - -	- - -	- - -
	LM-P-043C	- -	25	35	0	- - -	- - -	- - -	- - -	- - -	- - -
	LM-P-043D	- TR	35	25	0	- - -	- - -	- - -	- - -	- - -	- - -
	LM-P-043E	- -	65	10	0	- - -	- - -	- - -	- - -	- - -	- - -
	LM-P-043F	- -	45	30	0	- - -	- - -	- - -	- - -	- - -	- - -
	LM-P-043G	- -	15	20	0	- - -	- - -	- - -	- - -	- - -	- - -
	LM-P-043H	- -	20	20	0	- - -	- - -	- - -	- - -	- - -	- - -
	LM-P-043I	- -	15	25	0	- - -	- - -	- - -	- - -	- - -	- - -
	LM-P-043J	- -	25	20	0	- - -	- - -	- - -	- - -	- - -	- - -
1925L-Haulage	LM-P-043K	- -	15	25	0	- - -	- - -	- - -	- - -	- - -	- - -
	LM-P-043L	TR -	25	40	0	- - -	- - -	- - -	- - -	- - -	- - -
	LM-P-043M	- -	20	25	0	- - -	- - -	- - -	- - -	- - -	- - -
	LM-P-043N	- -	30	30	0	- - -	- - -	- - -	- - -	- - -	- - -
	LM-P-043O	- -	25	30	0	- - -	- - -	- - -	- - -	- - -	- - -
	LM-P-043P	- -	20	30	0	- - -	- - -	- - -	- - -	- - -	- - -
	LM-P-043Q	- -	20	20	0	- - -	- - -	- - -	- - -	- - -	- - -
	LM-P-044A	- -	5	30	3	3 0.1	0.5	- -	- TR	- -	- -
	LM-P-044B	- -	25	25	0	- - -	- - -	- - -	- - -	- - -	- - -
	LM-P-044C	- -	30	20	0	- - -	- - -	- - -	- - -	- - -	- - -
1700L-450RMK	LM-P-044D	- -	15	30	0	- - -	- - -	- - -	- - -	- - -	- - -
	LM-P-044E	- -	30	25	0	- - -	- - -	- - -	- - -	- - -	- - -
	LM-P-044F	- -	25	20	0	- - -	- - -	- - -	- - -	- - -	- - -
	LM-P-044G	- -	30	25	0	- - -	- - -	- - -	- - -	- - -	- - -
	LM-P-044H	- -	25	20	0	- - -	- - -	- - -	- - -	- - -	- - -
DDH4938	LM-P-045A	- -	40	TR	0	CONTACT NOT CAPTURED					
	LM-P-045B	- -	10	2	0	- - -	- - -	- - -	- - -	- - -	- - -
	LM-P-045C	- -	15	15	0	- - -	- - -	- - -	- - -	- - -	- - -
	LM-P-045D	- -	40	5	0	- - -	- - -	- - -	- - -	- - -	- - -
	LM-P-045E	- -	10	5	0	- - -	- - -	- - -	- - -	- - -	- - -
1700-RMK	LM-P-055A	- -	70	60	100	60	0.5	15	TR	-	25
	LM-P-055B	- -			28	21	0.1	7	TR	-	-
	LM-P-055C	TR -	35	60	0	- - -	- - -	- - -	- - -	- - -	- - -
	LM-P-055D	- -	25	20	0	- - -	- - -	- - -	- - -	- - -	- - -
	LM-P-055E	TR -	30	10	0	- - -	- - -	- - -	- - -	- - -	- - -
	LM-P-055F	- -	20	10	0	- - -	- - -	- - -	- - -	- - -	- - -
	LM-P-055G	- -	10	20	0	- - -	- - -	- - -	- - -	- - -	- - -
	LM-P-055H	- -	15	20	0	- - -	- - -	- - -	- - -	- - -	- - -
	LM-P-055I	- -	10	20	0	- - -	- - -	- - -	- - -	- - -	- - -
	LM-P-060A	- -	20	10	100	90	5	5	- -	- TR	- -
	LM-P-060B	15 -			20	18	-	1	TR	1	-
	LM-P-060C	- -			0	- - -	- - -	- - -	- - -	- - -	- - -
	LM-P-060D	1 -			0	- - -	- - -	- - -	- - -	- - -	- - -
	LM-P-060E	- -			0	- - -	- - -	- - -	- - -	- - -	- - -
	LM-P-060F	- -			0	- - -	- - -	- - -	- - -	- - -	- - -

Note: TR = trace.

picked, and checked for purity under a binocular microscope. Detailed sulphur isotope observations can be found in Table 3. $\delta^{34}\text{S}$ analyses at the G.G. Hatch Isotope Laboratories, Ottawa University, using combustion on a Flash Elemental analyzer with a DeltaPlus XP isotope ratio mass spectrometer coupled with a ConFlo IV (Table 3).

$^{40}\text{Ar}/^{39}\text{Ar}$ Geochronology

Field observations indicate that hydrothermal fluids precipitated actinolite crystals prior to chalcopyrite emplacement. Actinolite is not commonly targeted for $^{40}\text{Ar}/^{39}\text{Ar}$ dating (Fig. 5) due to its low potassium and high calcium content. However, in the absence of any other datable phase, dating of this actinolite was undertaken using a $^{40}\text{Ar}/^{39}\text{Ar}$ technique in an attempt to constrain the timing of the hydrothermal event. A hand sample was collected from an alteration rind that had developed along the contact of the massive chalcopyrite vein and grey gabbro. The sample was crushed, sieved to -60/+80 mesh, and processed through heavy liquid (methylene iodide) separation to segregate actinolite from chalcopyrite. Actinolite grains were hand-picked under a binocular microscope ($600\text{--}800\ \mu\text{m}$)

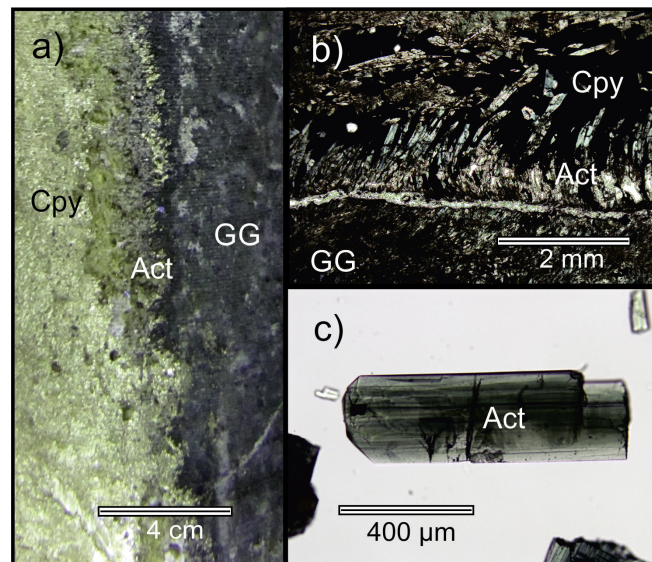


Figure 5. **a)** Drill core from drillhole FNX40272 showing the contact relationship of the grey gabbro (GG), the gem-quality actinolite (Act), and the sharp-walled chalcopyrite (Cpy); **b)** Sample LM-P-005 in plane polarized light showing a closer relationship between the chalcopyrite and the grey gabbro; **c)** Gem-quality actinolite crystals from sample LM-P-060 (plane polarized light with oil), which is from the sharp-walled vein contact.

Table 3. $\delta^{34}\text{S}$ analyses of chalcopyrite from levels 1700, 1850, 1925, and 2225, Podolsky deposit.

Sample ID	Mineralogy	$\delta^{34}\text{S}$ Value	Location	Host Rock	Mineral Texture	Comments
LM-PRC-01.1	chalcopyrite	4.37	1700-550 drift	grey gabbro	primary	sampled at beginning of sharp-walled chalcopyrite vein; trace amounts of actinolite present
LM-PRC-01.2	chalcopyrite	4.43	1700-550 drift	grey gabbro	primary	sampled at end of sharp-walled chalcopyrite vein; trace amounts of actinolite present
LM-PRC-01.3A	chalcopyrite	4.29	1700-550 drift	grey gabbro	primary	sampled at end of sharp-walled chalcopyrite vein; trace amounts of actinolite present
LM-PRC-01.3B	chalcopyrite	3.44	1700-550 drift	grey gabbro	primary	sampled at end of sharp-walled chalcopyrite vein; trace amounts of actinolite present
LM-PRC-02.1	chalcopyrite	4.35	1850-400 drift	grey gabbro	primary	sampled at beginning of sharp-walled chalcopyrite vein; trace amounts of magnetite present
LM-PRC-02.2	chalcopyrite	4.3	1850-400 drift	grey gabbro	primary	sampled in middle of sharp-walled chalcopyrite vein; trace amounts of magnetite present
LM-PRC-02.3	chalcopyrite	4.39	1850-400 drift	grey gabbro	primary	sampled at end of sharp-walled chalcopyrite vein; trace amounts of magnetite present
LM-PRC-03.1	chalcopyrite	4.5	1925-Haulage	grey gabbro	primary	sampled at beginning of sharp-walled chalcopyrite vein; trace amounts of magnetite present
LM-PRC-03.2	chalcopyrite	4.42	1925-Haulage	grey gabbro	primary	sampled in middle of sharp-walled chalcopyrite vein; trace amounts of magnetite present
LM-PRC-03.3	chalcopyrite	4.45	1925-Haulage	grey gabbro	primary	sampled in middle of sharp-walled chalcopyrite vein; trace amounts of magnetite present
LM-PRC-04.1A	chalcopyrite	4.32	2225-9450 drift	grey gabbro	primary	sampled at end of sharp-walled chalcopyrite vein; trace amounts of magnetite present
LM-PRC-04.1B	chalcopyrite	4.3	2225-9450 drift	grey gabbro	primary	sampled at beginning of sharp-walled chalcopyrite vein; trace amounts of magnetite present
LM-PRC-04.2	chalcopyrite	4.51	2225-9450 drift	grey gabbro	primary	sampled in middle of sharp-walled chalcopyrite vein; trace amounts of magnetite present
LM-PRC-04.3	chalcopyrite	4.28	2225-9450 drift	grey gabbro	primary	sampled in middle of sharp-walled chalcopyrite vein; trace amounts of magnetite present
LM-PRC-04.4	chalcopyrite	4.2	2225-9450 drift	grey gabbro	primary	sampled at end of sharp-walled chalcopyrite vein; trace amounts of magnetite present

and then subjected to a 15-minute ultrasonic bath in acetone, followed by several rinses with deionized water and ethyl alcohol to remove all traces of methylene iodide.

The actinolite grains were loaded into a 3 mm deep aluminum foil packet, which was subsequently loaded into a 35 mm vertical foil tube, stacked among other sample packets and placed into a tubular hole of an aluminum cylinder. Several packets containing grains of both the primary flux monitor PP-20 hornblende (equivalent to monitor Hb3gr, 1074 ± 5 Ma, 1σ ; Jourdan et al., 2006) and the secondary standard FCT-San (28.02 ± 0.16 1σ Ma; Renne et al., 1998) were interspersed among the packets. The prepared can was irradiated for 960 MWH in medium flux position 8C (cadmium-shielded) at the research nuclear reactor of McMaster University (MNR) in Hamilton, Ontario, Canada. Neutron flux was approximately 1.04×10^{13} neutrons/(cm²/s), at a 2.5 MW power level. Correction factors for typical interference species produced by thermal neutrons during irradiation are 0.003 (⁴⁰Ar/³⁹Ar_K), 0.0007 (³⁹Ar/³⁷Ar_{Ca}), and 0.00028 (³⁶Ar/³⁷Ar_{Ca}).

Upon return from the reactor, mineral grains and flux monitors were loaded into 1.5 mm diameter pits in a copper planchet and placed under vacuum in an all-metal extraction line. Conventional step-heating of grains was carried out using a Photon Machines Inc. Fusion 10.6 55W CO₂ laser coupled to the extraction line and analyzed with a Nu Instruments Noblesse multicollector noble gas mass spectrometer at the Geological Survey of Canada, Ottawa (see McDougall and Harrison (1999) for a complete description of conventional ⁴⁰Ar/³⁹Ar step-heating methodology). Laser heating was homogenized over a beam radius of 2 mm for a total of 40 seconds, after which the released gas was exposed to SAESTM NP-10 (~400°C) and HY-STOR® 201 (room temperature) getters in the extraction line for three minutes. Following gettering, sample gas was expanded into the mass spectrometer. Argon ions were measured with a fixed array of one Faraday (FAR) and three ETP® discrete dynode ion-counting multipliers (IC0, IC1, IC2) using the MC-O multicollection scheme described in Kellett and Joyce (2014). Blanks were run every 5th analysis, in an identical manner to unknowns. Relative collector efficiency and mass bias corrections were made for FAR, IC1, and IC2 collectors relative to IC0 using measurements of air; analyses of which were carried out periodically throughout the analytical sessions (see Kellett and Joyce (2014) for complete intercalibration details). Error in J-factor values are conservatively estimated at $\pm 1.0\%$ (2σ). Full results, including blank measurements, are included in Appendix C. Sensitivity of the Nu Noblesse at the time of analyses was 7.1–7.5

amps/mol. Data collection, reduction, error propagation, age calculation, and plotting were performed using the software Mass Spec (version 7.93) (Deino, 2001). In the discussion of analytical results, a ‘plateau’ is defined as three or more consecutive heating steps of the statistically same age (within 2σ) that, together, comprise greater than 50% of the total ³⁹Ar released. The plateau age would be calculated by weighting each included step by the inverse of the variance. The term ‘pseudoplateau’ refers to a plateau-like region from which an approximate age can be estimated. The integrated age (or total gas age), which appears on the release spectra, is calculated by weighting all the individual steps by the fraction of ³⁹Ar released. Ages presented in the step-heating release spectra are based on the assumption that atmospheric argon has a ⁴⁰Ar/³⁶Ar ratio of 298.56 (Lee et al., 2006). This atmospheric ratio can be verified by plotting data on an isotope correlation diagram. On inverse isochron diagrams, ³⁶Ar/⁴⁰Ar is plotted against ³⁹Ar/⁴⁰Ar for each analysis, after being corrected for both interfering isotopes and mass spectrometer intercalibration factors. A York (1969) linear least squares regression can be applied to the data, from which errors in both ratios and error correlations can be determined. A robust inverse isochron age is obtained when data points fall along a linear isochron, and the y-intercept yields the trapped non-radiogenic ⁴⁰Ar/³⁶Ar composition, and the x-intercept gives the ³⁹Ar/⁴⁰Ar, which is used to calculate the excess argon-corrected absolute age. Ages discussed in this report are at the 95% confidence level.

Results

The first ‘reconnaissance’ aliquot of actinolite fortuitously contained sufficient potassium and a manageable amount of calcium in the grain to carry the step-heating experiment to completion. The release spectrum for Aliquot 1 was somewhat noisy, with excess ⁴⁰Ar in step D, but the majority of the steps fell within the same age range (except step F), giving a pseudoplateau integrated age of 1890 ± 40 Ma (Fig. 6a). Additional aliquots were analyzed in hopes that a plateau might be obtained, the pseudoplateau age could be reproduced with higher precision, or a robust inverse isochron age could be achieved by using data points from multiple aliquots. A total of five step-heating aliquots were completed, the spectra for which are presented in Figure 6. Aliquots 1 and 2 were single-grains, whereas for aliquots 3, 4, and 5, multiple grains were heated simultaneously (4, 4, and 5 grains, respectively) in an attempt to increase the signal intensity and reduce the uncertainty of the ages. The gas-release, Ca/K, and Cl/K patterns were different for each aliquot, and none of the aliquots produced a plateau from which a robust age could be determined. These

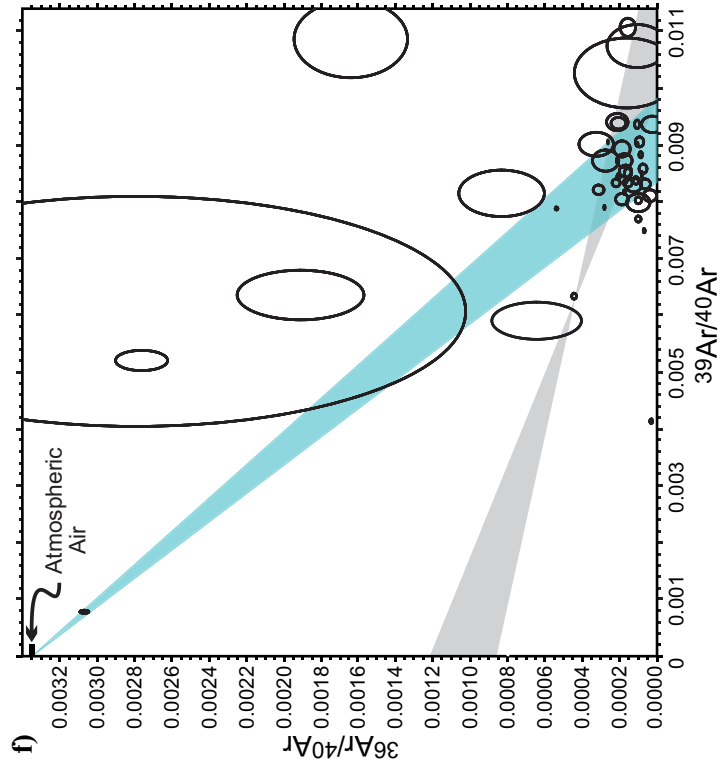
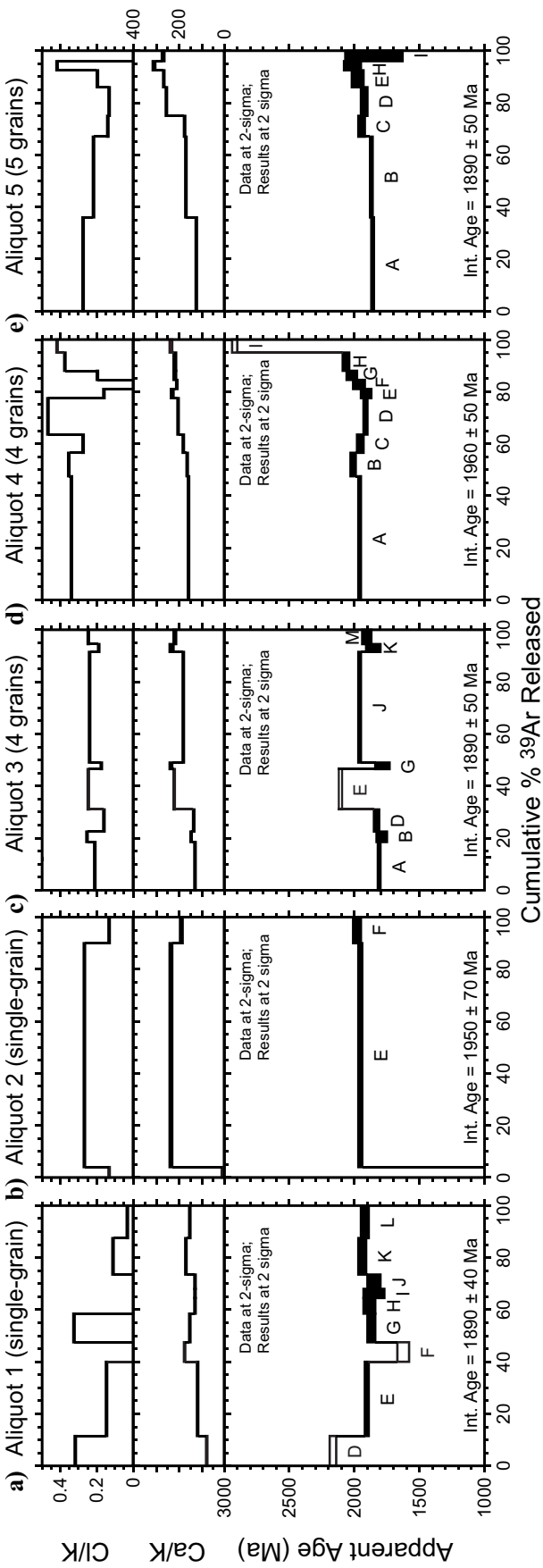
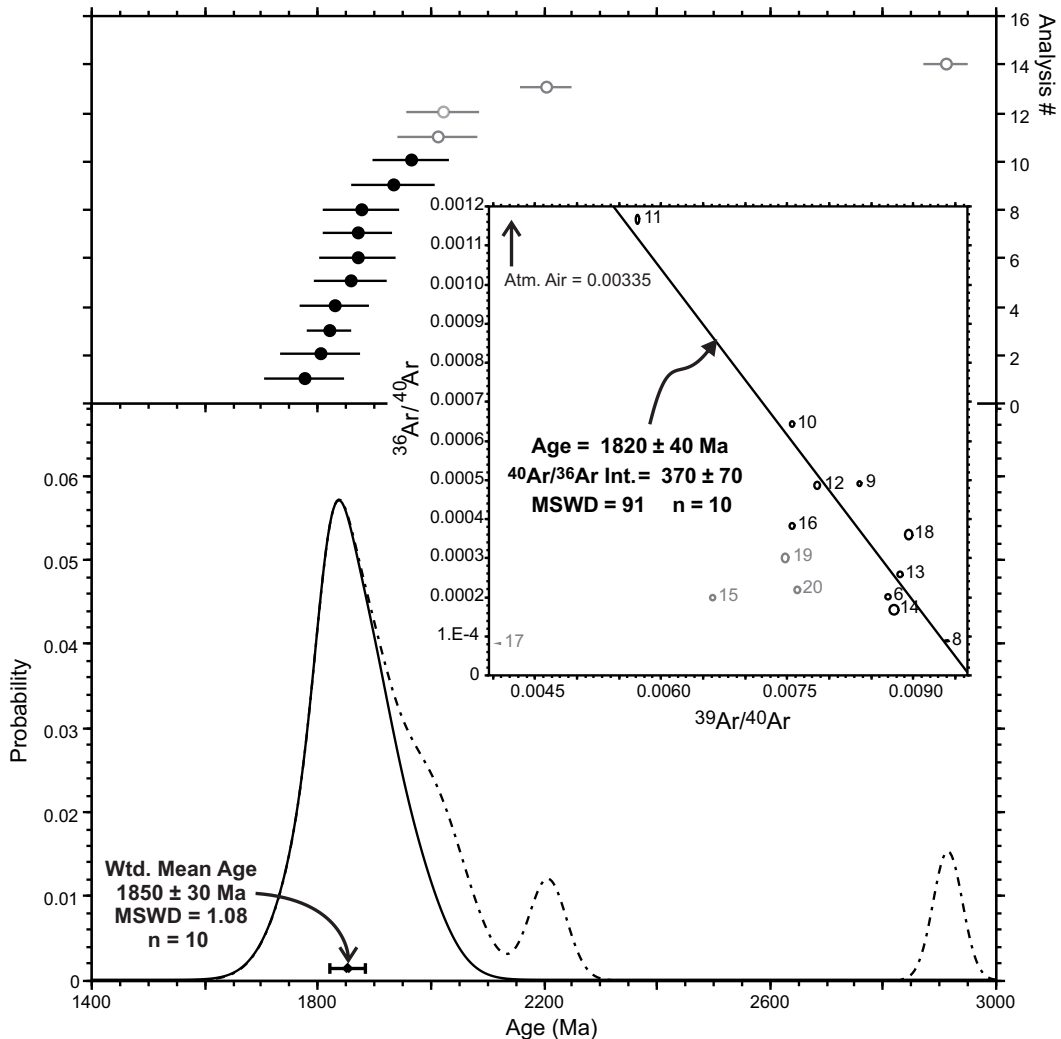


Figure 6. (a) to (e) Gas-release spectra for five aliquots of actinolite from sample LM-P-060. Only gas steps comprising >2% of the total ^{39}Ar are plotted. Integrated ages are shown for each aliquot, and do not include steps that are shown as unfilled boxes (or plot off-scale of the diagram, which step A does in Aliquot 2). (f) Inverse isochron plot showing data points for all five step-heated aliquots. Error ellipses are 2σ . The data neither cluster tightly nor do they fall along a linear trend, illustrating the heterogeneity of the composition of the argon trapped in the actinolite. The aqua band shows a range of possible regressions anchored by 1 near-atmospheric data point; ages derived from the $^{39}\text{Ar}/^{40}\text{Ar}$ x-intercepts range from ca. 1812 to 1990 Ma. The grey shaded areas are fields that fall between two example regressions for data points containing excess ^{40}Ar ; ages derived from these $^{39}\text{Ar}/^{40}\text{Ar}$ x-intercepts (corrected for excess ^{40}Ar) range from ca. 1510 to 1800 Ma (with $^{40}\text{Ar}/^{36}\text{Ar}$ compositions of 1160 ± 160 Ma and 820 ± 90 Ma, respectively). The data are too scattered to confidently determine an age for the actinolite crystallization from this inverse isochron diagram.

Figure 7. Age probability distribution plot of 14 single-fusion analyses of actinolite from sample LM-P-060. Error ellipses and values are 2σ . The most prominent peak, using 10 of the 14 analyses (rejected analyses are plotted as open circles), is at age 1850 ± 30 Ma. The dotted line shows the peaks of the rejected data. The inset shows the inverse isochron diagram of the 14 analyses. All analyses plotted below the atmospheric line (not shown because it falls outside the scale of the diagram), which suggests all analyses contained excess ^{40}Ar . The scatter of the data and the very high mean square weighted deviation (MSWD = 91) for the regression line through the 10 analyses that were used for the weighted mean age illustrates the highly variable composition of excess argon in these grains. A best estimate of the actinolite age (corrected for excess) would be 1820 ± 40 Ma, with a $^{40}\text{Ar}/^{36}\text{Ar}$ intercept of ~ 370 .



phenomena probably reflect intra- and intergrain compositional heterogeneity, and/or degassing of hydrothermal fluid inclusions of varying composition and abundance. The scatter of the data on the inverse isochron plot (Fig. 6f) also indicates that there are multiple compositions of excess argon with no justification for choosing one regression over another in order to assign an inverse isochron age.

In a final attempt to resolve the scattered age results, single fusions of 14 single-grain aliquots were carried out and examined to determine whether an age could be statistically reproduced. Integrated ages from Aliquots 6 through 20 are presented in an age-probability plot in Figure 7. A weighted mean age of 1850 ± 30 Ma was calculated based on 10 grains (MSWD= 1.08). All the grains analyzed contained varying amounts of excess ^{40}Ar (Fig. 7), and a regression through the 10 analyses used in the weighted mean calculation yields an imprecise age of 1820 ± 40 Ma (corrected for excess ^{40}Ar), which is within error of both the weighted mean age and of the Sudbury impact event (1849.53 ± 0.21 Ma; Davis, 2008).

SUMMARY

This report combines large-scale observations (i.e. remapping drill core logs and hand sample observations) and small-scale observations (petrography, whole rock geochemistry, isotopes coupled with argon geochronology on hydrothermal alteration) with chemical attributes of the fluid(s) responsible for alteration and mineralization. The knowledge gained from this research has highlighted the potential of far-field vectors to identify Cu-PGE mineralization in the richly mineralized Sudbury mining district.

ACKNOWLEDGMENTS

The authors would like to thank KGHM's Podolsky 2012-2013 team for their guidance, access, feedback, coordination, and insight with their computer programs, facilities, and logistics. This work was initiated and funded by the Targeted Geoscience Initiative 4 (TGI-4) program of the Geological Survey of Canada (GSC) within the Ni-Cu-PGE-Cr project and included support to the first author under the Research Affiliate Program 2012-2014 of the Natural Resources of Canada.

REFERENCES

- Ames, D.E. and Farrow, C.E.G., 2007. Metallogeny of the Sudbury mining camp, Ontario, *In* Mineral Deposits of Canada: A Synthesis of Major Deposit Types, District Metallogeny, the Evolution of Geological Provinces, and Exploration Methods (ed.) W.D. Goodfellow; Geological Association of Canada, Mineral Deposits Division, Special Publication 5, p. 329–350.
- Ames, D.E. and Houlé, M.G., 2011. Overview of the Targeted Geoscience Initiative 4 nickel-copper-platinum group elements-chromium project (2010–2015)—mafic to ultramafic ore systems: footprint, fertility and vectors, *In* Summary of Field Work and Other Activities 2011; Ontario Geological Survey, Open File Report 6270, p. 37-1 to 37-7.
- Ames, D.E., Dare, S.A., Hanley, J.J., Hollings, P., Jackson, S., Jugo, P.J., Kontak, D., Linnen, R., and Samson, I.M., 2012. Update on research activities in the Targeted Geoscience Initiative 4 magmatic-hydrothermal nickel-copper-platinum group elements ore system subproject: System fertility and ore vectors, *In* Summary of Field Work and Other Activities 2012; Ontario Geological Survey, Open File Report 6280, p. 41-1 to 41-11.
- Clayton, R.N. and Mayeda, T.K., 1963. The use of bromine pentafluoride in the extraction of oxygen from oxides and silicates for isotopic analysis; *Geochimica et Cosmochimica Acta*, v. 27, p. 43–52.
- Davis, D., 2008. Sub-million-year age resolution of Precambrian igneous events by thermal extraction-thermal ionization mass spectrometer Pb dating of zircon: Application to crystallization of the Sudbury impact melt sheet; *Geology*, v. 36, p. 383–386.
- Deino, A.L., 2001. User's manual for Mass Spec v. 5.02; Berkeley Geochronology Center Special Publication 1a, p. 119.
- Farrow, C.E.G., Everest, J.O., King, D.M., and Jolette, C., 2005. Sudbury Cu-(Ni)-PGE systems: Refining the classification using McCreedy West mine and Podolsky project case studies, *In* Exploration for Platinum-Group Elements Deposits, (ed.) J.E. Mungall; Mineralogical Association of Canada, Short Course Series, v. 35, p. 163–180.
- Jourdan, F., Verati, C., and Féraud, G., 2006. Intercalibration of the Hb₃gr $^{40}\text{Ar}/^{39}\text{Ar}$ dating standard; *Chemical Geology*, v. 231, p. 177–189.
- Kellett, D. and Joyce, N., 2014. Analytical details of single- and multicollection $^{40}\text{Ar}/^{39}\text{Ar}$ measurements for conventional step-heating and total fusion age calculation using the Nu Noblesse at the Geological Survey of Canada; *Geological Survey of Canada*, Technical Note 8, 27 p. doi:10.4095/293465
- Krogh, T.E., Davis, D.W., and Corfu, F., 1984. Precise U-Pb zircon and baddeleyite ages for the Sudbury area, *In* Geology and Ore Deposits of the Sudbury Structure, (eds.) E.G. Pye, A.J. Naldrett, and P.E. Giblin; Ontario Geological Survey, Special Volume 1, p. 431–446.
- Lee, J.-Y., Marti, K., Severinghaus, J.P., Kawamura, K., Yoo, H.-S., Lee, J.B., and Kim, J.S., 2006. A redetermination of the isotopic abundances of atmospheric Ar; *Geochimica et Cosmochimica Acta*. v. 70, p. 4507–4512.
- Mattinson, J.M., 2005. Zircon U-Pb chemical abrasion (“CA-TIMS”) method: combined annealing and multi-step partial dissolution analysis for improved precision and accuracy of zircon ages; *Chemical Geology*, v. 22, p. 47–66.
- McDougall, I. and Harrison, T.M., 1999. *Geochronology and Thermochronology by the $^{40}\text{Ar}/^{39}\text{Ar}$ Method*; Oxford University Press.
- Renne, P.R., Swisher, C.C., Deino, A.L., Karner, D.B., Owens, T.L., and DePaolo, D., 1998. Intercalibration of standards, absolute ages and uncertainties in $^{40}\text{Ar}/^{39}\text{Ar}$ dating; *Chemical Geology*, v. 145, p. 117–152.
- York, D., 1969. Least squares fitting of a straight line with correlated errors; *Earth and Planetary Science Letters* 5, p. 320–324.